JCB Journal of Cell Biology

ARTICLE

Depolarization induces nociceptor sensitization by $Ca_V1.2$-mediated PKA-II activation

Jörg Isensee[1], Marianne van Cann[1], Patrick Despang[2], Dioneia Araldi[3], Katharina Moeller[1], Jonas Petersen[4], Achim Schmidtko[4], Jan Matthes[2], Jon D. Levine[3], and Tim Hucho[1]

Depolarization drives neuronal plasticity. However, whether depolarization drives sensitization of peripheral nociceptive neurons remains elusive. By high-content screening (HCS) microscopy, we revealed that depolarization of cultured sensory neurons rapidly activates protein kinase A type II (PKA-II) in nociceptors by calcium influx through $Ca_V1.2$ channels. This effect was modulated by calpains but insensitive to inhibitors of cAMP formation, including opioids. In turn, PKA-II phosphorylated Ser1928 in the distal C terminus of $Ca_V1.2$, thereby increasing channel gating, whereas dephosphorylation of Ser1928 involved the phosphatase calcineurin. Patch-clamp and behavioral experiments confirmed that depolarization leads to calcium- and PKA-dependent sensitization of calcium currents ex vivo and local peripheral hyperalgesia in the skin in vivo. Our data suggest a local activity-driven feed-forward mechanism that selectively translates strong depolarization into further activity and thereby facilitates hypersensitivity of nociceptor terminals by a mechanism inaccessible to opioids.

Introduction

Decades of research detailed a central role of cAMP-dependent protein kinase A (PKA) for activity-driven pre- and postsynaptic plasticity in neurons. Key events surrounding the activation of PKA are depolarization-triggered calcium influx, Ca^{2+}/calmodulin (CaM)–dependent activation of adenylyl cyclases (ACs), and production of intracellular cAMP (Kandel, 2001; Korte and Schmitz, 2016). In concert with other kinases, PKA then increases transmitter release as well as the gating and trafficking of voltage-gated calcium channels (VGCCs), leading to increased pre- and postsynaptic activity (Greengard, 2001; Kandel, 2001; Korte and Schmitz, 2016). Similar plastic changes also occur at synapses of primary afferent sensory neurons and their respective secondary neurons in the dorsal horn of the spinal cord. This phenomenon may lead to central sensitization (Latremoliere and Woolf, 2009), a state in which the central nervous system response to peripheral nociceptive sensory input is amplified (Henrich et al., 2015; Sandkühler, 2009).

In contrast to processes at spinal synapses, peripheral terminals of nociceptive sensory neurons lack neuronal synaptic input. Instead, depolarizing inputs are generated by sensors for noxious thermal, mechanical, or chemical stimuli (Basbaum et al., 2009; Hucho and Levine, 2007; Kuner and Flor, 2016), accompanied by substantial calcium influx into nociceptors (Chen et al., 2019). These nociceptive sensors in peripheral nerve terminals of nociceptors are highly plastic (Basbaum et al., 2009; Hucho and Levine, 2007). In particular, stimulation of various metabotropic receptors activates PKA, resulting in nociceptor sensitization (Aley and Levine, 1999; Bavencoffe et al., 2016; Liao et al., 1999; Song et al., 2006; Villarreal et al., 2009). However, whether electrical activity of nociceptors can drive PKA activation and thereby PKA-dependent peripheral hypersensitivity remains unexplored.

Recently, we identified a conformation-sensitive antibody that selectively binds to domains of regulatory RII subunits that become accessible after type II PKA (PKA-II) activation (Isensee et al., 2014a; Isensee et al., 2018). This antibody allows quantifying endogenous PKA-II activity in nociceptors. Previously, we used this method in combination with high-content screening (HCS) microscopy–based quantification to study G protein–coupled receptor (GPCR)–mediated pro- and anti-nociceptive signaling in nociceptors (Isensee et al., 2014a; Isensee and Hucho, 2019; Isensee et al., 2018; Isensee et al., 2017a; Isensee et al., 2017b; Isensee et al., 2014b). Using this approach, we found that $Ca_V1.2$ mediates depolarization-induced PKA-II activity in nociceptors and identified a feed-forward mechanism of cAMP-independent regulation of $Ca_V1.2$ by PKA-II. Further molecular

[1]Department of Anesthesiology and Intensive Care Medicine, Translational Pain Research, Faculty of Medicine and University Hospital of Cologne, University of Cologne, Cologne, Germany; [2]Department of Pharmacology, Faculty of Medicine and University Hospital of Cologne, University of Cologne, Cologne, Germany; [3]Division of Neuroscience, Departments of Medicine and Oral & Maxillofacial Surgery, University of California, San Francisco, San Francisco, CA; [4]Institute for Pharmacology and Clinical Pharmacy, Goethe University Frankfurt, Frankfurt am Main, Germany.

Correspondence to Jörg Isensee: joerg.isensee@uk-koeln.de; Tim Hucho: tim.hucho@uk-koeln.de.

biological, genetic, electrophysiological, and behavioral experiments support that depolarization drives PKA-mediated mechanical hypersensitivity by $Ca_V1.2$. This experimental series may be of considerable interest, as a functional role of $Ca_V1.2$ in nociceptors remains elusive and neuronal activity has not been described so far as a mechanism to induce mechanical hyperalgesia in primary afferent nociceptors (North et al., 2018). Of note, this feed-forward phenomenon appears to be unresponsive to classical analgesics such as opioids.

Results

Depolarization induces transient PKA-II signaling in nociceptors

We took advantage of an antibody that binds to the phosphorylated inhibitory sites of PKA-II regulatory subunits RIIα and RIIβ (collectively referred to as pRII; Zhang et al., 2015; Zhang et al., 2012) only in dissociated, active PKA-II kinases. This allows monitoring of the activity of endogenous PKA-II in primary sensory neurons expressing the neuronal marker ubiquitin C-terminal hydrolase L1 (UCHL1, formerly PGP9.5; Isensee et al., 2018) using an automated HCS microscopy approach (Fig. 1 A; Isensee et al., 2014a; Isensee and Hucho, 2019; Isensee et al., 2018; Isensee et al., 2017a; Isensee et al., 2017b; Isensee et al., 2014b).

Rat dorsal root ganglion (DRG) neurons were depolarized by KCl (Ataman et al., 2016; Greer and Greenberg, 2008; Kim et al., 2010). KCl depolarization resulted in a transient increase in pRII intensity, indicating induction of PKA-II activity (Fig. 1 B). KCl dose–response curves were steep, with half-maximal effective concentrations (EC_{50}s) of 10 mM in neurons of rats or mice (Figs. 1 C and S1 A), suggesting that PKA activation requires substantial changes of the membrane potential. PKA-II activation was not restricted to depolarization by KCl and also observed after depolarization with the selective voltage-gated sodium channel (VGSC; Na_v) toxin veratridine (Fig. 1 D). PKA-II activity occurred predominantly in smaller neurons expressing nociceptor markers such as the PKA regulatory subunit RIIβ, the VGSC $Na_V1.8$, or the calcitonin gene–related peptide (CGRP), but not in neurofilament 200 (NF200)–expressing mechano- and proprioceptors (Fig. 1, E–I; and Fig. S1, B–D; Isensee et al., 2014a). This suggests that neuronal depolarization activates PKA-II predominantly in nociceptive DRG neurons.

Depolarization-induced PKA-II activity mediated by calcium influx through L-type VGCCs

Depolarization-induced activation of PKA may involve several classes of voltage- and ligand-gated channels. DRG neurons express the VGCC isoforms $Ca_V1.2$ (L-type), $Ca_V2.1$ (P/Q-type), $Ca_V2.2$ (N-type), and $Ca_V3.2$ (T-type; Dolphin, 1991; Fossat et al., 2010; Gadotti et al., 2015; Zamponi, 2016; Zamponi et al., 2015), which has been confirmed by RNA sequencing (RNA-seq) experiments of our laboratory on mouse and rat DRG cultures (Fig. 2 A; Isensee et al., 2014b) and public single-cell RNA-seq data of mouse DRG neurons (Fig. 2 B; Zeisel et al., 2018). Furthermore, VGSCs, ligand-gated transient receptor potential (TRP) channels, or NMDA-type glutamate receptors can be involved in depolarization (Bourinet et al., 2014).

We explored the mechanism underlying depolarization-induced PKA-II activation in sensory neurons. Treatment with lidocaine, a potent broad-spectrum inhibitor of VGSCs, did not affect KCl-induced activation of PKA-II (Fig. S2 A). Similarly, the selective NMDA receptor antagonist D-AP5, the $Ca_v3.1$-3 blocker TTA-P2, and a combination of the $Ca_v2.1$-2 blocker ω-agatoxin IVA, ω-conotoxin MVIIC, and ω-conotoxin GVIA did not inhibit the pRII response to KCl depolarization (Fig. 2 C). The pRII response remained also unchanged in mice lacking two of the main TRP channels expressed in sensory neurons, TRPV1 and TRPA1 (Fig. S2 B).

By contrast, blocking Ca_V1 VGCCs with the two structurally unrelated blockers verapamil and diltiazem dose-dependently inhibited the pRII response to KCl with half-maximal inhibitory concentrations (IC_{50}s) of 16 µM and 37 µM, respectively (Fig. 2, D–G, red versus green line). (S)-(-)-Bay K 8644, a positive modulator of Ca_V1 VGCCs, substantially increased and prolonged the pRII response to a low dose of 10 mM KCl (Fig. 2 H). This effect of Bay K 8644 was dose dependent, with an EC_{50} value of 80 nM (Fig. 2 I), supporting involvement of Ca_V1.

Activation of PKA-II requires calcium influx into Ca_V1 nanodomains

To corroborate dependence on calcium channels, we tested whether calcium is the PKA-II–activating factor, if this requires Ca_V1 channels, and if other calcium routes may effectively activate PKA-II as well. Chelation of extracellular calcium with EGTA completely abolished the pRII response (Fig. 2 J). Using the cell-permeable chelator BAPTA-AM, we explored the relevance of intracellular calcium. In presence of BAPTA-AM, depolarization still activated PKA-II at early time points, suggesting that PKA-II activation depends on local calcium at the calcium channel (Fig. 2 K). Therefore, calcium entry at a distant site by pore-forming ionomycin should not activate PKA-II. Indeed, stimulation with ionomycin led to substantial calcium influx, as shown by CA5 calcium imaging (Fig. S2 C), but had a minimal effect on activation of PKA-II (Fig. S2 D). These findings support that induction of PKA-II by depolarization requires calcium changes in nanodomains near Ca_V1 channels (Tadross et al., 2013).

Knockout of $Ca_V1.2$ in $NaV1.8^+$ nociceptors reduces PKA-II activity

There are four L-type VGCCs, $Ca_V1.1$–1.4. Our transcriptome data indicate substantially higher expression levels of $Ca_V1.2$ compared with other L-type channel isoforms in DRGs (Fig. 2 A). Consistent with predominant depolarization-induced PKA-II activation in nociceptive neurons (Fig. S1), published single-cell RNA-seq data find $Ca_V1.2$ mostly in nociceptors but not in mechano- and proprioceptors (NF1-3) or tactile C-low-threshold mechanoreceptors (NP1; Fig. 2 B; Zeisel et al., 2018). $Ca_V1.2$ is also coexpressed with $Na_V1.8$ (Scn10a) in nociceptive neurons (Fig. 3 A). Accordingly, we bred $Na_V1.8$-Cre mice (Agarwal et al., 2004) with floxed $Ca_V1.2$ mice (Seisenberger et al., 2000) to knock out $Ca_V1.2$ in $Na_V1.8^+$ nociceptors (Fig. 3 B). At 8 wk of age, $Na_V1.8^{Cre/+}$/$Cacna1c^{fl/fl}$ mice (cKO) showed no obvious abnormalities. Expression of the neuronal marker UCHL1 and the

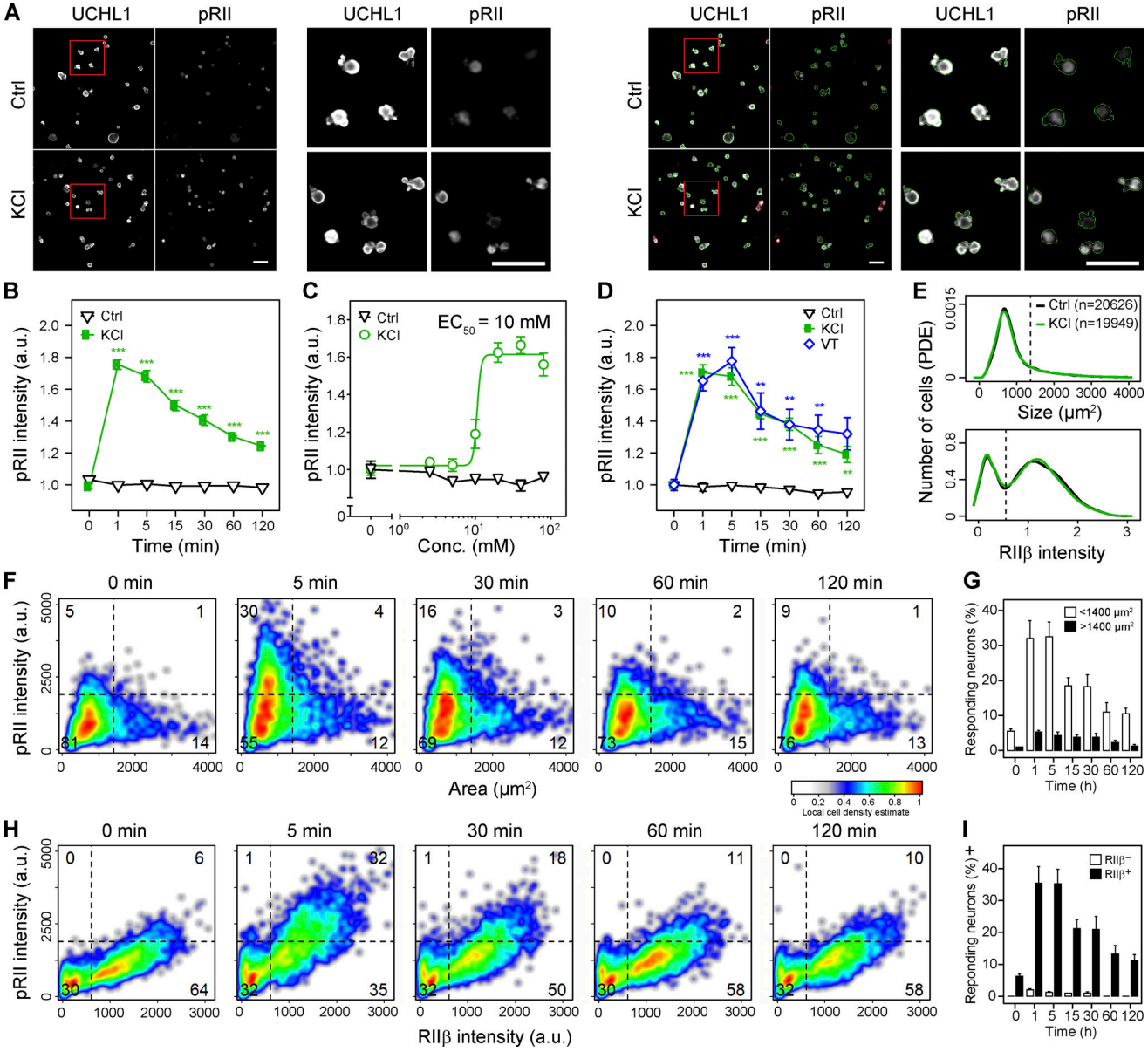

Figure 1. **Depolarization activates PKA-II in nociceptive neurons. (A)** HCS microscopy images of rat DRG neurons stimulated with solvent (Ctrl) or KCl (40 mM) for 1 min. Cultures were immunolabeled with UCHL1 to identify the neurons and pRII to quantify PKA-II signaling activity. Red frames mark enlarged image sections; green or red encircled neurons in the left panel indicate the mask to selected or rejected objects, respectively (see Materials and methods). Scale bars, 100 µm. **(B)** Time course of pRII intensity in DRG neurons stimulated with KCl (40 mM). **(C)** Dose–response curve of pRII intensity in DRG neurons exposed to KCl (0–80 mM, EC_{50} = 10 mM) for 3 min. **(D)** Time course of pRII intensity in DRG neurons treated with veratridine (VT; 100 µM) to open VGSCs in comparison to the KCl (40 mM) response. **(E)** Size and RIIβ intensity distributions of control and KCl-stimulated DRG neurons used to determine the gating thresholds for the following subgroup analysis. PDE, phosphodiesterase. **(F)** Cell density plots showing single-cell data of pRII intensities versus the neuronal areas of KCl (40 mM)–stimulated sensory neurons. Dashed lines indicate gating thresholds used to calculate the percentage of cells in the respective quadrant. Combined data of *n* = 4 experiments with a total of >3,000 neurons per condition. **(G)** Quantification of responding smaller (<1,400 µm²) and larger (>1,400 µm²) neurons in *n* = 4 replicate experiments with a total of >3,000 neurons per condition. **(H)** Cell density plots showing single-cell data of pRII versus RIIβ intensities in the same neurons shown in F. **(I)** Quantification of responding $RII\beta^-$ and $RII\beta^+$ neurons. HCS data in B–D are means ± SEM; *n* = 3–4 independent experiments; >2,000 neurons/condition; two-way ANOVA with Bonferroni's test; **, P < 0.01; ***, P < 0.001 indicate significance levels between baseline and stimulated conditions at the respective time point.

nociceptor marker RIIβ was unchanged (Fig. 3, C and D), as was the total number of viable neurons after overnight culture (Fig. 3 E). Quantifying $Ca_V1.2$-specific immunofluorescence intensity averaged over all nociceptive and nonnociceptive neurons, we observed a significant reduction in $Ca_V1.2$ intensity (Fig. 3 F). Compensatory up-regulation of other Ca_Vs such as $Ca_V1.3$ has been reported (Xu et al., 2003). Indeed, the signal reduction was less pronounced in neurons from cKO mice when we used a pan-Ca_V1 antibody, which also detects $Ca_V1.3$ (Fig. S3 A).

To test for a role of $Ca_V1.2$ in PKA-II activation, we measured the effect of conditional $Ca_V1.2$-deficiency on PKA-II activity (pRII) in nociceptive ($RII\beta^+$) and nonnociceptive ($RII\beta^-$) neurons.

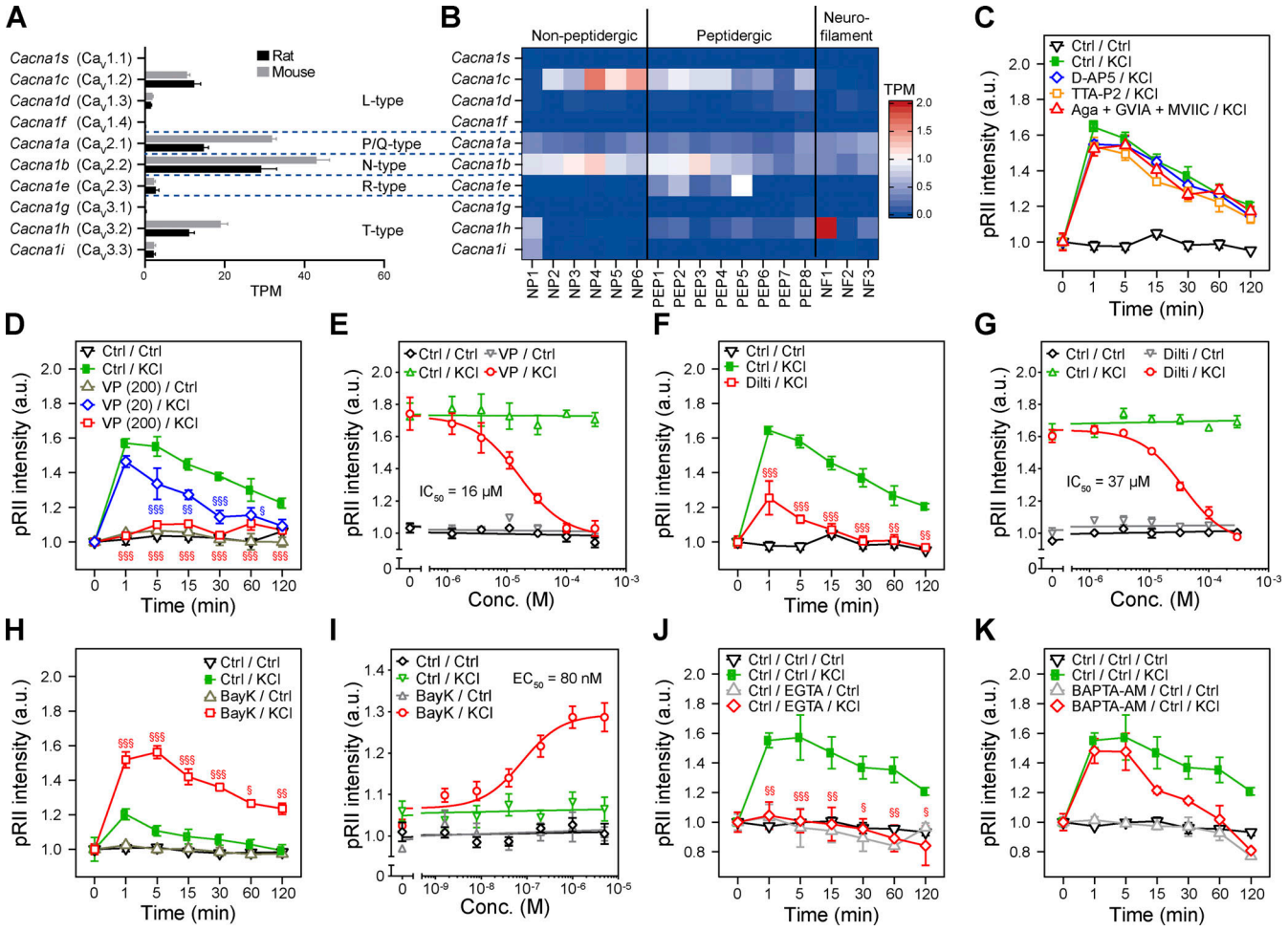

Figure 2. **Calcium influx through $Ca_V1.2$ induces PKA-II activity during depolarization. (A)** Expression pattern of VGCC α subunits in overnight cultures of rat and mouse DRG determined by RNA-seq (Isensee et al., 2014b). TPM, transcripts per kilobase million. **(B)** Expression pattern of VGCC α subunits in mouse DRG neuron subgroups determined by single-cell RNA-seq (Zeisel et al., 2018). **(C)** Time course of pRII intensity in KCl-depolarized rat sensory neurons after pretreatment (10 min) with the NMDA receptor antagonist D-AP5 (10 µM), the Cav3.1-3.3 blocker TTA-P2 (1 µM), and a combination of the Cav2.1/2.2 blocker ω-agatoxin IVA (100 nM), ω-conotoxin MVIIC (200 nM), and ω-conotoxin GVIA (1 µM). **(D)** Inhibitory effect of verapamil (20 or 200 µM, 10-min pretreatment) on the pRII increase induced by KCl depolarization. **(E)** Dose–response curve showing the effect of verapamil (0–200 µM; IC_{50} = 16 µM) on pRII signals induced by KCl depolarization (3 min). **(F)** Inhibitory effect of diltiazem (100 µM, 10 min) on the KCl-induced pRII increase. **(G)** Dose–response curve showing the inhibition of KCl-induced pRII signals by diltiazem (0–200 µM; IC_{50} = 37 µM). **(H)** Reinforcing effect of the Ca_V1 agonist (S)-(-)-Bay K 8644 (2 µM, 10 min) on pRII signals induced by a low dose of KCl (10 mM). **(I)** Dose–response curve showing the reinforcing effect of Bay K 8644 (0–5 µM; EC_{50} = 80 nM) on pRII signals induced by KCl (10 mM, 3 min). **(J)** Chelation of extracellular calcium with EGTA (2.5 mM, 30-min prestimulation) abolished the pRII response to KCl-depolarization. **(K)** Effect of the cell-permeable calcium chelator BAPTA-AM (100 µM, 60 min) on pRII signals induced by KCl depolarization (compound effect: $F_{1,28}$ = 10.9, P < 0.003). Values in C–K represent means ± SEM; *n* = 3–4 experiments; >2,000 neurons/condition; two-way ANOVA with Bonferroni's test; §, P < 0.05; §§, P < 0.01; §§§, P < 0.001 indicate significance levels between KCl-induced pRII signals in the absence or presence of an agonist/antagonist.

Indeed, only in nociceptive neurons did we observed a significant reduction of the baseline (Fig. 3 G) and KCl-induced pRII (Fig. 3 H). In line with a role of $Ca_V1.2$ for PKA-II activation, also pretreating the neurons with increasing doses of (S)-(-)-Bay K 8644 before stimulation with a low dose of KCl (10 mM) had a reduced effect in neurons of cKO mice (Fig. 3 I). At doses up to 200 nM, the induction of PKA-II activity was lost in cKO mice (Fig. 3 J).

Adenoviral knockdown of $Ca_V1.2$ reduces PKA-II activity

While supporting a role of $Ca_V1.2$ for PKA-II activity, the changes in the conditional knockout animals were of limited size. This may be due to developmental compensation by up-regulation of $Ca_V1.3$ (Xu et al., 2003) and/or only partial Cre recombination (Harno et al., 2013). Therefore, in a separate approach, we transduced cultured DRG neurons of adult mice with capsid-modified adeno-associated viruses (AAVs; AAV-PHP.S; Chan et al., 2017) to express a validated $Ca_V1.2$-specific knockdown shRNA (Michels et al., 2018) along with a GFP reporter. Indeed, 1 wk (8 days in vitro [div]) and 2 wk (15 div) after transduction, >60% of DRG neurons expressed GFP (Fig. 4, A–C). $Ca_V1.2$-specific (Fig. 4, D and E) and pan-Ca_V1 (Fig. S3, B and C) immunofluorescence intensities were both significantly reduced in GFP^+, but not GFP^-, neurons, indicating down-regulation of $Ca_V1.2$. Corroborating the observations in cKO mice, $Ca_V1.2$ down-regulation led to reduced basal and depolarization-induced PKA-II activity at 1 wk (Fig. 4 F) that was more pronounced

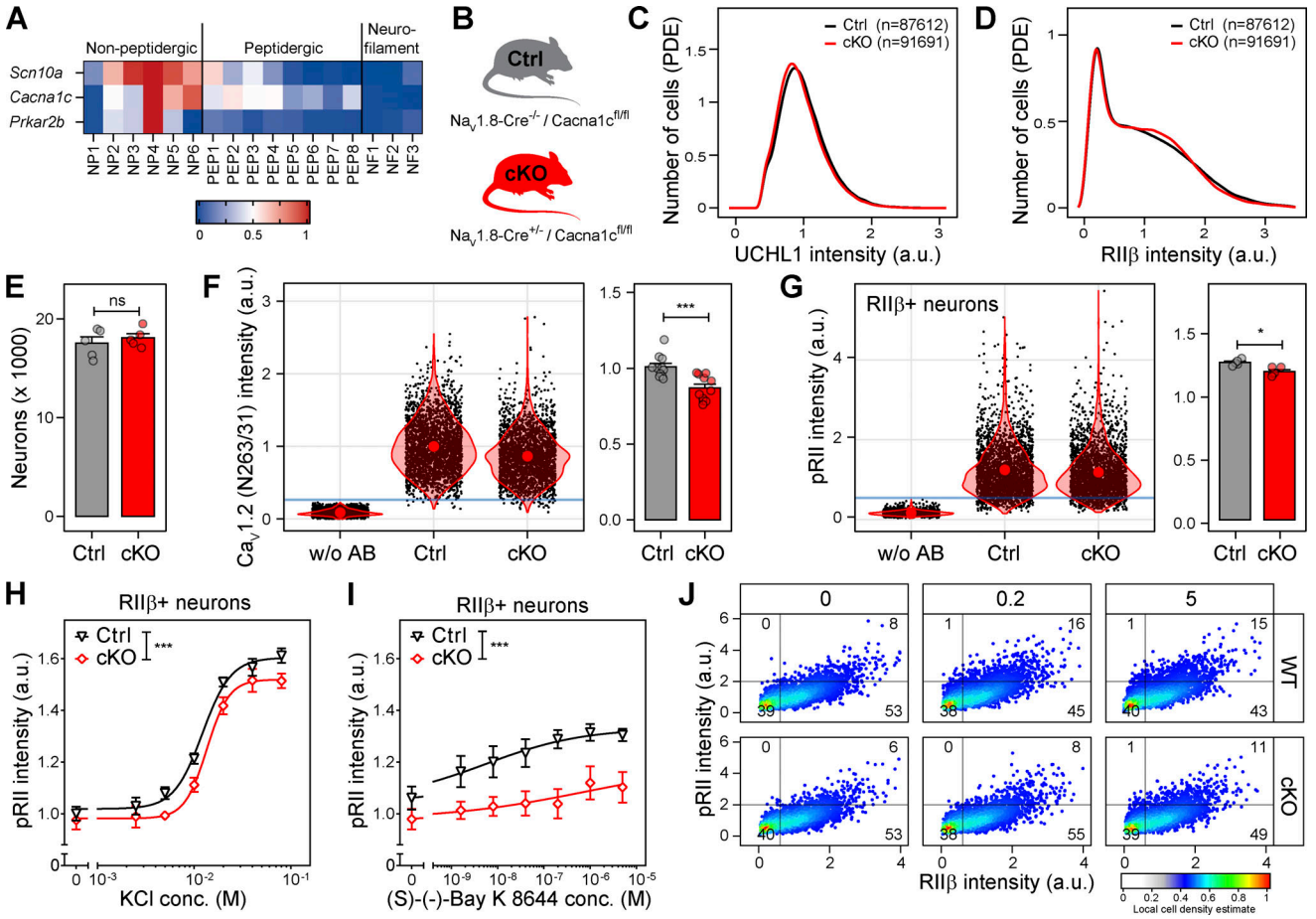

Figure 3. **Deletion of Ca$_V$1.2 in NaV1.8$^+$ nociceptors reduces PKA-II activity. (A)** Expression pattern of Na$_V$1.8 (Scn10a), Ca$_V$1.2 (Cacna1c), and RIIβ (Prkar2b) in subgroups of DRG neuron determined by single-cell RNA-seq (Zeisel et al., 2018). **(B)** Conditional mouse model to delete Ca$_V$1.2 in Na$_V$1.8-expressing DRG neurons. **(C and D)** Distribution of UCHL1 and RIIβ expression levels in DRG neurons of cKO mice and respective controls lacking Cre recombinase (Ctrl). **(E)** Total numbers of viable DRG neurons after overnight culture determined by HCS microscopy (n = 3 females and 2 males per genotype). **(F)** Single-cell data and mean intensities obtained using a Ca$_V$1.2-specific antibody (clone N263/31) indicating down-regulation of Ca$_V$1.2 (n = 10 cultures from three mice per genotype, >6,000 neurons per genotype, Student's t test). The primary antibody was omitted in respective controls (w/o AB). **(G)** Basal genotype difference of pRII intensity in all solvent stimulated RIIβ$^+$ control neurons (n = 3 females and 2 males per genotype, >15,000 neurons/condition, Student's t test). **(H)** Dose-dependent induction of pRII intensity by KCl (0–80 mM) in cKO and Ctrl mice (n = 3 females and 2 males per genotype; genotype effect: $F_{4,62}$ = 5.6, extra-sum-of-squares F test). **(I)** Dose-dependent induction of pRII intensity by 10 mM KCl after 10 min preincubation with (S)-(-)-Bay K 8644 (0–5 µM) in cKO and Ctrl mice. (n = 3 females and 2 males per genotype; genotype effect: $F_{4,62}$ = 13.9, extra-sum-of-squares F test). **(J)** Single-cell data of selected condition shown in I. Values in G–I are means ± SEM; *, P < 0.05; ***, P < 0.001.

2 wk after transduction (Fig. 4, G and H). In conclusion, the pharmacological, genetic, and molecular biological data support that Ca$_V$1.2 mediates depolarization-induced activation of PKA-II.

Depolarization-induced activation of PKA-II is cAMP independent

Our data indicate that local calcium influx through Ca$_V$1.2 activates PKA-II. Next, we explored the activating mechanism. Calcium can activate the Ca^{2+}/CaM-stimulated AC isoforms AC1, AC3, and AC8, resulting in cAMP formation and PKA activation (Alexander et al., 2013). This signaling pathway essentially contributes to neuroplastic changes in various pain processing brain areas after nerve injury (Sharif-Naeini and Basbaum, 2011; Wang et al., 2011; Wei et al., 2002; Wei et al., 2006). Accordingly, selective AC1 inhibitors such as NB001 and ST034307 showed analgesic effects in pain models in vivo (Brust et al., 2017; Wang et al., 2011).

The calcium-dependent ACs AC1, AC3, and AC8 are expressed in DRG, according to our transcriptome data (Fig. S4 A). However, HCS microscopy analyses revealed that preincubation with high doses of the inhibitors NB001 or ST034307 did not inhibit the increase of pRII after depolarization (Fig. S4, B and D). These inhibitors did not inhibit the response to 5-HT, which is mediated by G$_s$-coupled 5-HT$_4$ receptors rather than calcium in sensory neurons (Fig. S4, C and E; Isensee et al., 2017a). AC5, an AC inhibited by calcium signaling (Alexander et al., 2013), has been reported to be essential for pain relief by opioids and relevant for nociception in acute and chronic pain models (Kim et al., 2007; Kim et al., 2006). Inhibition of AC5/6 with SQ22536 or NKY80 (Brand et al., 2013), however, also failed to block the pRII response to KCl (Fig. S4, F and H). Of note, SQ22536 inhibited the Gα$_s$-mediated PKA-II activation by 5-HT (Fig. S4 G).

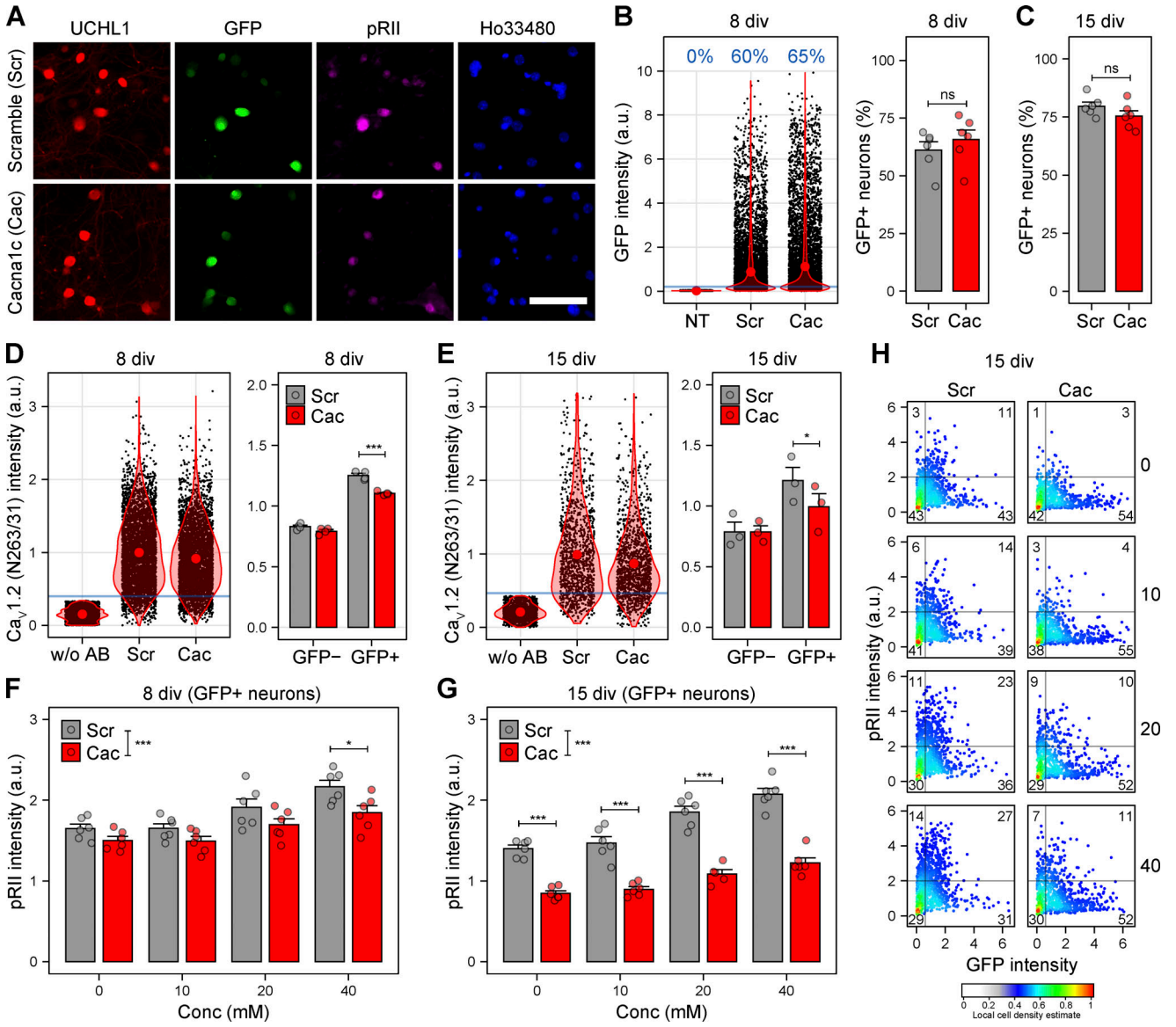

Figure 4. **Adenoviral knockdown of $Ca_V1.2$ reduces PKA-II activity. (A)** Representative HCS microscopy images of mouse DRG neurons transduced with AAV-PHP.S-U6-shRNA:Scramble-CAG-GFP (Scr) or AAV-PHP.S-U6-shRNA:Cacna1c-CAG-GFP (Cac) to knock down $Ca_V1.2$. Neurons were transduced after overnight culture (1 div) and fixed 1 wk (8 div) or 2 wk (15 div) later. Cultures were immunolabeled for the neuronal marker UCHL1 and pRII to quantify PKA-II signaling activity. The expression of GFP indicated efficient transduction. Nuclei were stained with Hoechst 34580. Scale bar, 100 µm. **(B and C)** GFP expression levels in individual neurons (left) and mean numbers of GFP^+ neurons after 8 div (n = 6, >6,000 neurons per condition, Student's t test) as well as after 15 div (n = 6, total of >1,000 neurons per condition, Student's t test). **(D and E)** Single-cell data of all analyzed neurons (left) and mean intensities in GFP^- and GFP^+ neurons (right) obtained using a $Ca_V1.2$-specific antibody (clone N263/31) at 8 div (D; n = 4, >4,000 neurons) and 15 div (E, n = 3, >1200 neurons) indicating down-regulation of $Ca_V1.2$ in GFP+ neurons. The primary antibody was omitted in respective controls (w/o AB). **(F and G)** Effect of AAV-mediated $Ca_V1.2$ knockdown on pRII intensity levels induced by 3-min stimulation with KCl at 8 div (F; n = 6, >6,000 neurons, two-way ANOVA with Bonferroni's test) and 15 div (G, n = 6, >1,000 neurons per condition). **(H)** Cell density plots showing single-cell data of pRII intensities versus GFP expression after 15 div as shown in G. Values in B–G are means ± SEM; *, P < 0.05; ***, P < 0.001.

Inability of AC inhibitors to block depolarization-induced PKA-II activity may be due to ineffective entry into neurons. To circumvent this, we applied opioids to activate endogenous inhibitory G_i-coupled opioid receptors. Opioids efficiently decrease PKA-II activity induced by 5-HT or forskolin in sensory neurons (Isensee et al., 2017a). Nevertheless, coapplication of fentanyl, oxycodone, or [Leu^5]-enkephalin did not decrease depolarization-induced PKA-II activity (Fig. 5 A).

As neither pharmacological- nor receptor-mediated inhibition of AC reduced depolarization-induced PKA-II activity, we tested whether cAMP is involved at all. We applied the unselective phosphodiesterase inhibitor 3-isobutyl-1-methylxanthine (IBMX) to block cAMP degradation. If cAMP is involved, then the presence of IBMX should result in accumulation of cAMP and thereby amplification of the response. As reported previously (Isensee et al., 2017b), pretreatment with IBMX increased and prolonged the GPCR-mediated

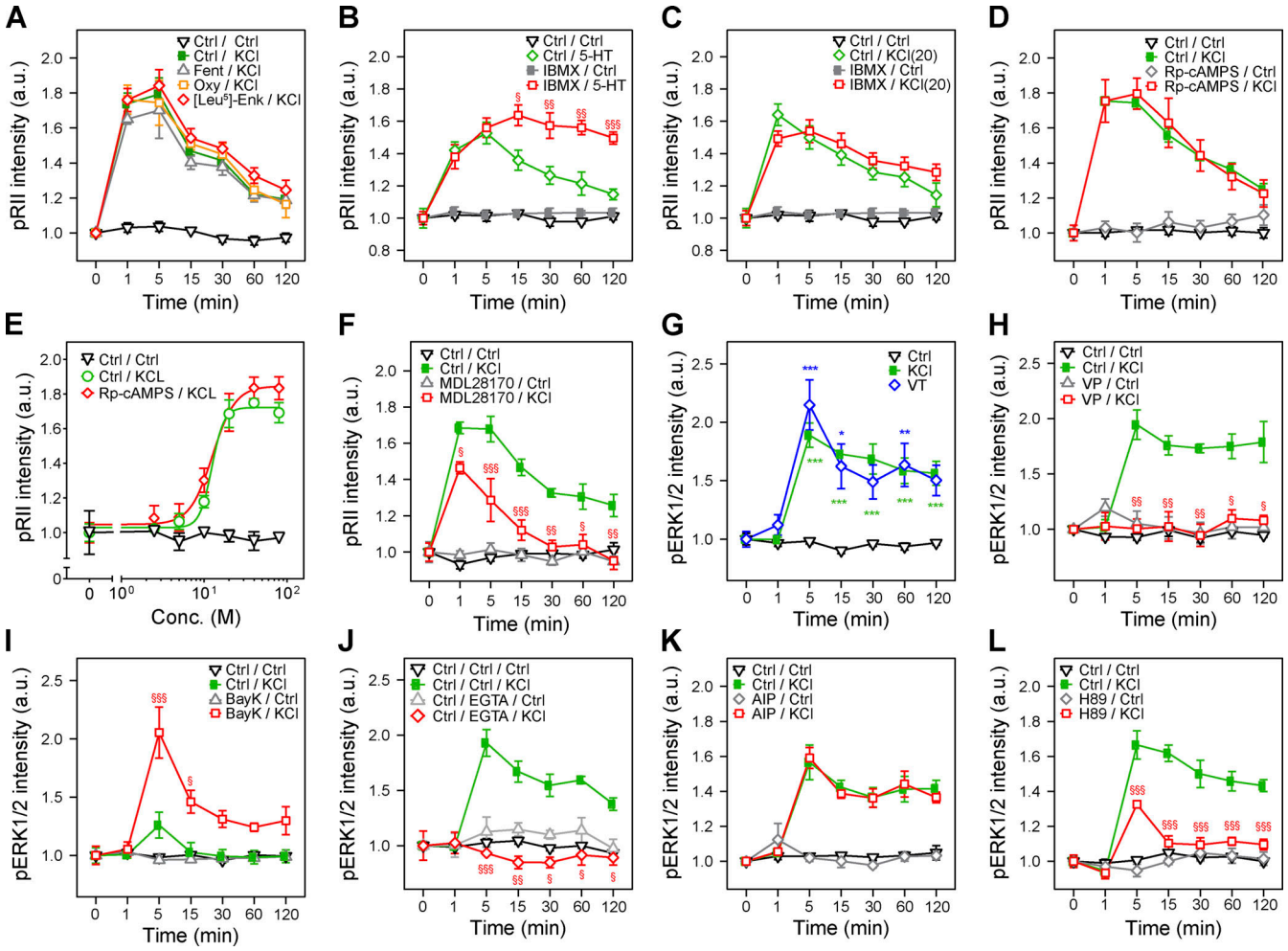

Figure 5. **KCl-induced PKA-II activity is cAMP independent but modulated by calpains. (A)** The pRII increase induced by KCl (40 mM) was not inhibited by fentanyl (Fent; 10 µM), oxycodone (Oxy; 10 µM), or [Leu^5]-enkephalin (Enk; 10 µM) in rat sensory neurons. **(B and C)** Effect of the phosphodiesterase inhibitor IBMX (100 µM, 30-min pretreatment) on the pRII increase induced by 5-HT (250 nM) or KCl (40 mM). Fig. S4, J and K show not-normalized data indicating basal elevation of pRII intensity by IBMX. **(D and E)** The cAMP antagonist Rp-cAMPS-pAB (10 µM) has no effect on the induction of pRII intensity by KCl (40 mM). **(F)** Effect of the calpain inhibitor MDL28170 (100 µM, 30 min) on the pRII increase by KCl (40 mM). **(G)** Time course of pERK1/2 intensity in DRG neurons treated with veratridine (VT; 100 µM) to open VGSCs in comparison to the KCl (40 mM) response. **(H)** Inhibitory effect of verapamil (VP; 200 µM, 10 min pretreatment) on ERK1/2 phosphorylation induced by depolarization (40 mM KCl). **(I)** The pERK1/2 response to a low dose of KCl (10 mM) is reinforced by (S)-(-)-Bay K 8644 (2 µM, 10 min). **(J)** Chelation of extracellular calcium with EGTA (2.5 mM, 30 min) prevents the pERK1/2 increase. **(K)** The CaMKII inhibitor AIP (1 µM, 30 min) does not inhibit the induction of pERK1/2 by depolarization. **(L)** Pretreatment with the PKA inhibitor H89 (25 µM, 30 min) reduces the pERK1/2 response to KCl. Values represent means ± SEM; n = 3–4 experiments; >2,000 neurons/condition; two-way ANOVA with Bonferroni's test; §, $P < 0.05$; §§, $P < 0.01$; §§§, $P < 0.001$ indicate significance levels between KCl-induced pRII signals in the absence or presence of an inhibitor.

activation of PKA-II by 5-HT (Figs. 5 B and S4 J). However, the response to depolarization by KCl was unchanged (Figs. 5 C and S4 K), suggesting that cAMP is not involved in depolarization-mediated PKA activation. To further investigate this hypothesis, we applied a novel highly cell-permeable Rp-isomer of adenosine-3′, 5′-cyclic monophosphorothioate (Rp-cAMPS-pAB; Chepurny et al., 2013; Isensee et al., 2018; Schwede et al., 2015), which stabilizes the inactive state of the PKA holoenzyme and acts as a competitive cAMP antagonist (Bacskai et al., 1993; Badireddy et al., 2011; Gjertsen et al., 1995; Prinz et al., 2006; Rothermel et al., 1983). Notably, Rp-cAMPS-pAB did not inhibit depolarization-induced PKA-II activity (Fig. 5, D and E), supporting a cAMP-independent mechanism.

Induction of PKA-II activity is not sensitive to inhibitors of CaMKII or ERK1/2

As we found that depolarization-induced PKA-II activity is apparently cAMP independent, we tested whether kinases activated by calcium influx through $Ca_V1.2$ channels might represent upstream signaling events. Although the spatiotemporal order of signaling events is not yet fully elucidated, binding of Ca^{2+} to CaM tethered to the C-terminal tail of $Ca_V1.2$ channels has been implicated in the activation of Ca^{2+}/CaM-dependent protein kinase II (CaMKII) and ERK1/2 in neurons (Dolmetsch et al., 2001; Wheeler et al., 2008; Wheeler et al., 2012; Zühlke et al., 1999; Zühlke et al., 2000). Inhibition of CaMKII, which is directly activated by Ca^{2+}/CaM, decreases the early phase of depolarization-induced CREB phosphorylation,

whereas the inhibition of mitogen-activated protein kinase kinases (MEK) affects the late phase compatible with the suggestion that activation of a local pool of CaMKII is an initial upstream signaling event (Ma et al., 2014; Malik et al., 2014; Wheeler et al., 2008; Wu et al., 2001).

Blocking of CaMKII with KN93, but also with its inactive control derivative, KN92, reduced the pRII response to KCl depolarization in DRG neurons, indicating an off-target effect (Fig. S5, A and B). Indeed, both compounds are known to inhibit L-type VGCCs (Gao et al., 2006). Also, the more specific CaMKII inhibitor autocamtide-2–related inhibitory peptide (AIP) was ineffective, making an involvement of CaMKII in the pRII response unlikely (Fig. S5 C). In addition, the MEK inhibitor U0126 did not change the kinetic or dose dependency of PKA-II activity after KCl depolarization (Fig. S5, D and E), although U0126 effectively blocked depolarization-induced ERK1/2 phosphorylation (Fig. S5 F). Thus, our pharmacological data suggest that neither CaMKII nor MEK is involved in depolarization-induced activation of PKA-II.

The calpain inhibitor MDL 28170 reduces PKA-II activity after depolarization

Reports of cAMP-independent activation of PKA are rare (Brennan et al., 2006; Burgoyne et al., 2015; Dulin et al., 2001; Shell and Lawrence, 2012; Zhong et al., 1997). Interestingly, the regulatory RII subunits of PKA-II are substrates of calcium-activated cysteine proteases of the calpain family, which potentially modulate PKA activity (Shell and Lawrence, 2012). In neurons, calpains have been associated with memory formation such as vesicle exocytosis and morphological changes of synapses (Baudry et al., 2011). Calpains cleave the core and distal C terminus of the pore-forming α subunit of activated $Ca_V1.2$, a process called mid-channel proteolysis, which is believed to reduce channel activity (De Jongh et al., 1996; Hell et al., 1996; Hulme et al., 2006b; Michailidis et al., 2014). In addition, a recent transcriptome analysis of pain-associated brain regions identified a role of calpains for neuropathic pain in mice (Descalzi et al., 2017). We therefore preincubated sensory neurons with the calpain inhibitor MDL 28170 followed by depolarization. MDL 28170 significantly reduced the induction of PKA-II activity (Fig. 5 F), suggesting a potential role of proteolytic activity in modulating the activation of PKA-II after depolarization.

Depolarization induces PKA-dependent phosphorylation of ERK1/2

To verify that the increased pRII signal indeed reflects an increase in PKA activity, we tested for the phosphorylation of known PKA-dependent downstream signaling events. In other neurons, calcium influx during depolarization induces activity of the MAPK cascade (Dolmetsch et al., 2001; Impey et al., 1998; Rosen et al., 1994; Rosen and Greenberg, 1996). We previously showed that PKA-II activity induced by GPCR agonists results in PKA-dependent ERK1/2 activity in sensory neurons (Isensee et al., 2017b). To corroborate depolarization-induced activation of PKA-II, we depolarized the cells and analyzed for PKA-dependent phosphorylation of ERK1/2. Depolarization by KCl or veratridine led to approximately twofold higher levels of pERK1/2 (Fig. 6 G). The induction of pERK1/2 was inhibited by verapamil and increased in the presence of Bay K8644 (Fig. 6, H and I). Chelation of extracellular calcium with EGTA abolished the response, supporting that calcium entry through $Ca_V1.2$ channels is required (Fig. 5 J). In line with our previous reports, the increase in pERK1/2 was absent after 1-min stimulation, indicating a slower onset compared with PKA-II (Fig. 1 B versus Fig. 5 F). To delineate the mechanism, we found that H89 and U0126, but not AIP, effectively inhibited the pERK1/2 response, indicating that phosphorylation of ERK1/2 is downstream of PKA and MEK in sensory neurons (Fig. 6, K and L; and Fig. S5 F).

$Ca_V1.2$ activity is regulated by PKA-dependent phosphorylation of Ser1928

Previous studies revealed that PKA phosphorylates the intracellular C terminus of $Ca_V1.2$ at Ser1928 and thereby increases channel gating (De Jongh et al., 1996; Gao et al., 1997; Hall et al., 2007; Hofmann et al., 2014; Hulme et al., 2006a; Kamp and Hell, 2000; Mitterdorfer et al., 1996; Weiss et al., 2013) and that Ser1928 is dephosphorylated by Ca^{2+}-activated calcineurin, leading to channel inactivation (Dittmer et al., 2014; Xu et al., 2016).

We therefore tested for a potential feed-forward mechanism of depolarization-induced and $Ca_V1.2$-mediated activation of PKA, which in turn may phosphorylate $Ca_V1.2$ itself and thereby further increase depolarization-induced currents. After depolarization, we applied a phospho-specific antibody detecting Ser1928 phosphorylation of $Ca_V1.2$ ($pCa_V1.2$; Fig. 6, A and B). Supporting the specificity of the $pCa_V1.2$ antibody, we found a significant correlation of $pCa_V1.2$ and $Ca_V1.2$ signals (Fig. 6 C). Depolarization increased the $pCa_V1.2$ immunoreactivity in sensory neurons (Fig. 6 D). This increase was sensitive to verapamil (Fig. 6 D), whereas the overall $Ca_V1.2$ signal was not significantly affected (Fig. 6 E). The C terminus of $Ca_V1.2$ potentially acts as transcriptional regulator (Gomez-Ospina et al., 2006). Accordingly, we detected $pCa_V1.2$ immunoreactivity also in the nuclei of sensory neurons (Fig. 6 B). To study nuclear translocation, we modified the image analysis to quantify signal intensities in nuclear versus cytoplasmic regions of the neurons (Fig. 6 B). Following depolarization, $pCa_V1.2$ signals increased in the cytoplasm and with a slight delay also in the nucleus (Fig. 6, F and G). The increase of pCaV1.2 signals was sensitive to H89 and prolonged by the calcineurin inhibitor FK506, corroborating that PKA drives phosphorylation of $Ca_V1.2$ (Fig. 6, H and I). Accordingly, blocking the catalytic activity of PKA by the ATP-site inhibitor H89 effectively inhibited the pRII response to KCl at all analyzed time points and doses (Fig. 6, J and K). This indicates a feed-forward mechanism of $Ca_V1.2$-dependent calcium influx, PKA activation, and PKA-mediated increase in $Ca_V1.2$ activity.

Repetitive depolarization induces calcium and PKA-dependent sensitization of calcium currents in DRG neurons

To corroborate that depolarization of sensory neurons results in calcium and PKA-dependent sensitization of calcium channels in sensory neurons, we performed whole-cell patch-clamp

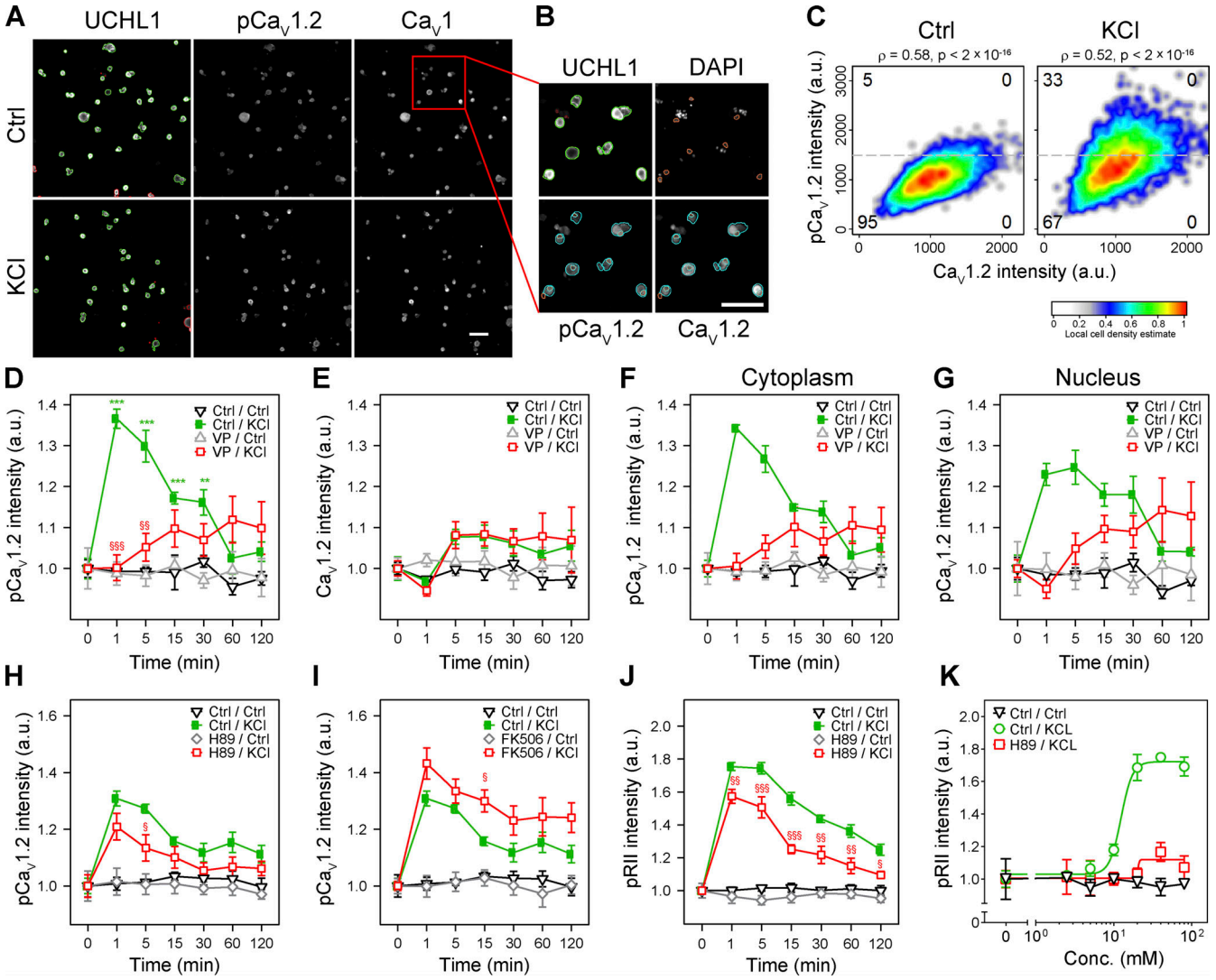

Figure 6. **PKA-dependent phosphorylation of Ser1928 regulates $Ca_V1.2$ gating. (A)** Representative images of rat DRG neurons stimulated with solvent (Ctrl) or KCl (40 mM) for 1 min. Cultures were labeled for UCHL1 to identify the neurons, phospho-Ser1928 of $Ca_V1.2$ ($pCa_V1.2$), and Ca_V1 channels (Ca_V1, clone L57/46). Green or red encircled objects indicate automatically selected or rejected objects, respectively. Scale bar, 100 µm. **(B)** Enlarged section demonstrating the modified image analysis to quantify in nuclear (orange) and cytoplasmic (blue) regions of neurons (green). **(C)** Cell density plots of single-cell data of $pCa_V1.2/Ca_V1$-labeled neurons stimulated with solvent control (Ctrl) or KCl (40 mM) for 1 min. The Spearman's rank correlation coefficient (ρ) and its P value are shown. **(D)** Depolarization (40 mM KCl) induces $Ca_V1.2$ phosphorylation, which is inhibited by verapamil (VP; 200 µM, 10 min). **(E)** The Ca_V1 intensity is unchanged after depolarization. **(F and G)** KCl-induced increase of $pCa_V1.2$ intensity in cytoplasmic versus nuclear regions. **(H)** Effect of the PKA inhibitor H89 on the $pCa_V1.2$ increase induced by depolarization. **(I)** Effect of the calcineurin inhibitor FK506 on the of $pCa_V1.2$ increase induced by depolarization. **(J)** Inhibitory effect of the PKA inhibitor H89 (25 µM, 30 min) on the pRII increase induced by depolarization. **(K)** Dose–response of KCl (0–80 mM) in the absence or presence of H89 (25 µM, 30 min). Data in D–J represent means ± SEM; *n* = 3–4 experiments; >2,000 neurons/condition; two-way ANOVA with Bonferroni's test; **, P < 0.01; ***, P < 0.001 indicate significance levels between baseline and stimulated conditions; §, P < 0.05; §§, P < 0.01; §§§, P < 0.001 indicate significance levels between the absence and presence of an agonist/antagonist.

electrophysiology recordings before and after applying a train of depolarization events (10 1-s-long test potentials to 0 mV). In the presence of calcium, we found a left shift of the I-V curve and significant reduction of the half-point for voltage dependence of activation ($V0.5_{act}$) 60 s after the depolarizing events, indicating sensitization of calcium channels (Fig. 7 A). This effect was calcium dependent since the left shift was absent when calcium was replaced with barium (Fig. 7 B). Preincubation of the neurons with H89 prevented the left shift in the presence of calcium (Fig. 7 C). Our data therefore corroborate that repetitive depolarization leads to calcium- and PKA-dependent sensitization of calcium currents.

Depolarization induces mechanical hyperalgesia in vivo

To understand the role of depolarization-induced signal transduction at a more physiological level, we performed intradermal injections of KCl into the hindpaw of rats and analyzed the effect on the mechanical nociceptive threshold (percentage reduction from baseline, Fig. 8 A; nociceptive threshold, Fig. 8 C). In line with our cellular data showing depolarization-induced

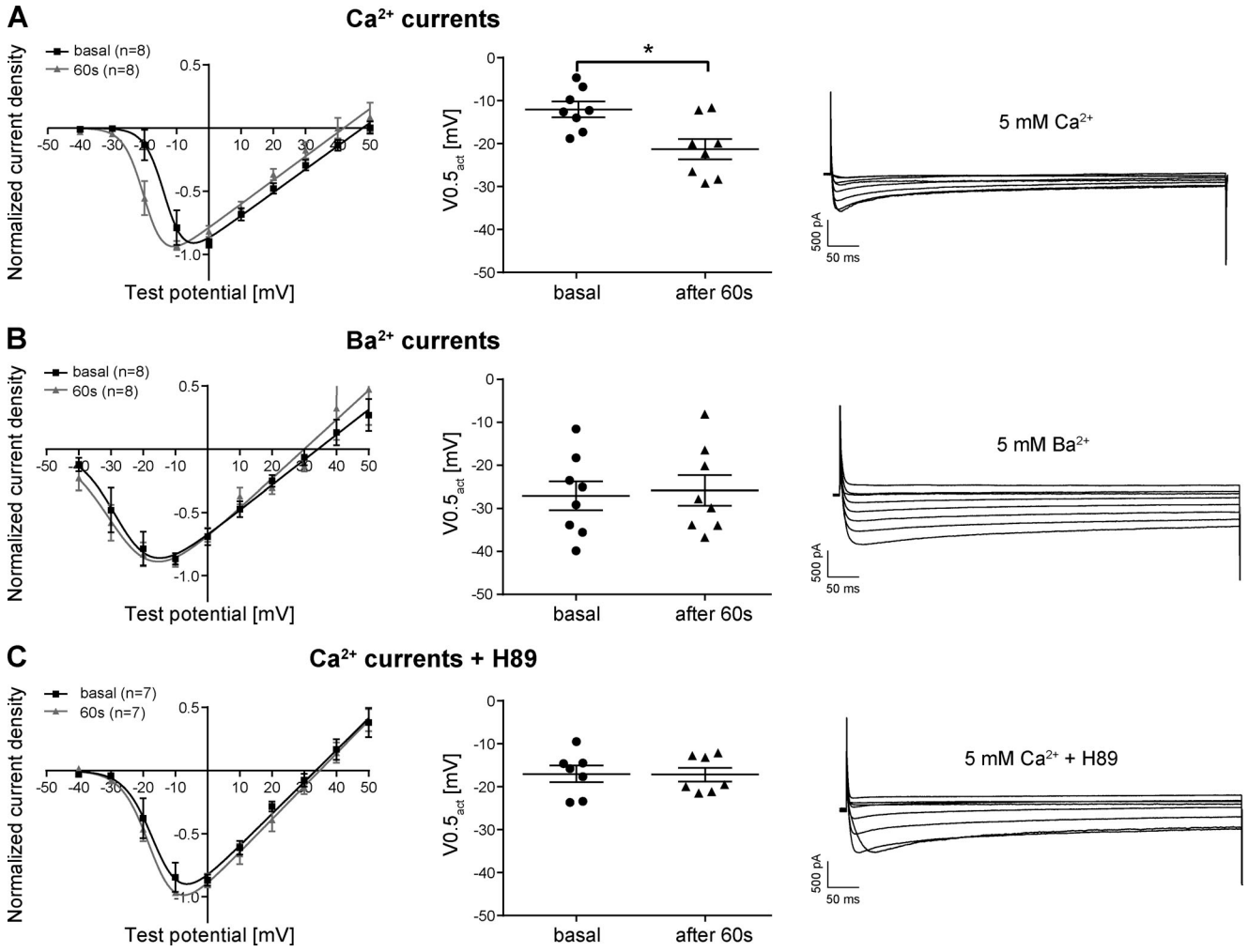

Figure 7. **Repetitive depolarization induces calcium and PKA-dependent sensitization of calcium currents in small diameter rat DRG neurons.** **(A)** Normalized I-V curves, $V0.5_{act}$, and representative traces for calcium currents (ICa) before and 60 s after applying a train of 10 1-s-long depolarizations to 0 mV. **(B)** Normalized I-V curves, $V0.5_{act}$, and representative traces for barium currents (IBa) before and 60 s after applying a train of 10 1-s-long depolarizations to 0 mV. **(C)** Normalized I-V curves, $V0.5_{act}$, and representative traces for calcium currents (ICa) before and 60 s after applying a train of 10 1-s-long depolarizations to 0 mV. DRG neurons were preincubated with H89 (25 µM, 1 h). Numbers of analyzed neurons are given in parentheses. Data represent means ± SEM of at least three animals. Currents underlying the I-V curves were elicited from −40 to +50 mV in 10-mV increments with 5 mM Ca^{2+} or Ba^{2+} as charge carrier. The holding potential was −90 mV. Paired *t* test; *, $P < 0.05$.

activation of sensitizing PKA signaling, we observed induction of a persistent (5 min to 6 h) robust mechanical hyperalgesia apparent as a reduction in the nociceptive threshold of 30% (Fig. 8, A and B). Consistent with our in vitro findings and supporting the hypothesis that local calcium influx initiates local sensitization signaling in the primary neuron, sensitization was not apparent in the contralateral paw (Fig. 8 A and Fig. 8 C). Further corroborating the local nature of the sensitization and the dependence on $Ca_V1.2$, depolarization-induced sensitization of the nociceptive threshold was blocked by local intradermal injection of verapamil (percentage reduction from baseline, Fig. 8 B; nociceptive threshold, Fig. 8 D).

Discussion

PKA is the longest known kinase, and electrical activity-driven modulation of synaptic connectivity of neurons is one of the core topics of neuroscience. Nevertheless, it remained unaddressed whether depolarization leads to PKA-dependent peripheral sensitization in nociceptive neurons lacking synaptic input. Quantification of thousands of sensory neurons by a single-cell–based HCS microscopy and the development of the first detection method of the activity state of endogenous PKA-II in cells allowed us to address this important topic (Isensee et al., 2014a; Isensee et al., 2018; Isensee et al., 2017a; Isensee et al., 2017b). Using KCl depolarization as well-accepted model to study depolarization-induced signal transduction (Ataman et al., 2016; Greer and Greenberg, 2008; Kim et al., 2010), our findings reveal that $Ca_V1.2$ channels mediate depolarization-induced activation of PKA-II in nociceptors (Fig. 9). In particular, we investigated how depolarization-induced calcium influx through $Ca_V1.2$ channels (1) activates intracellular kinase signaling, leading to (2) PKA-mediated regulation of electrophysiological calcium channel activity and (3) depolarization-induced

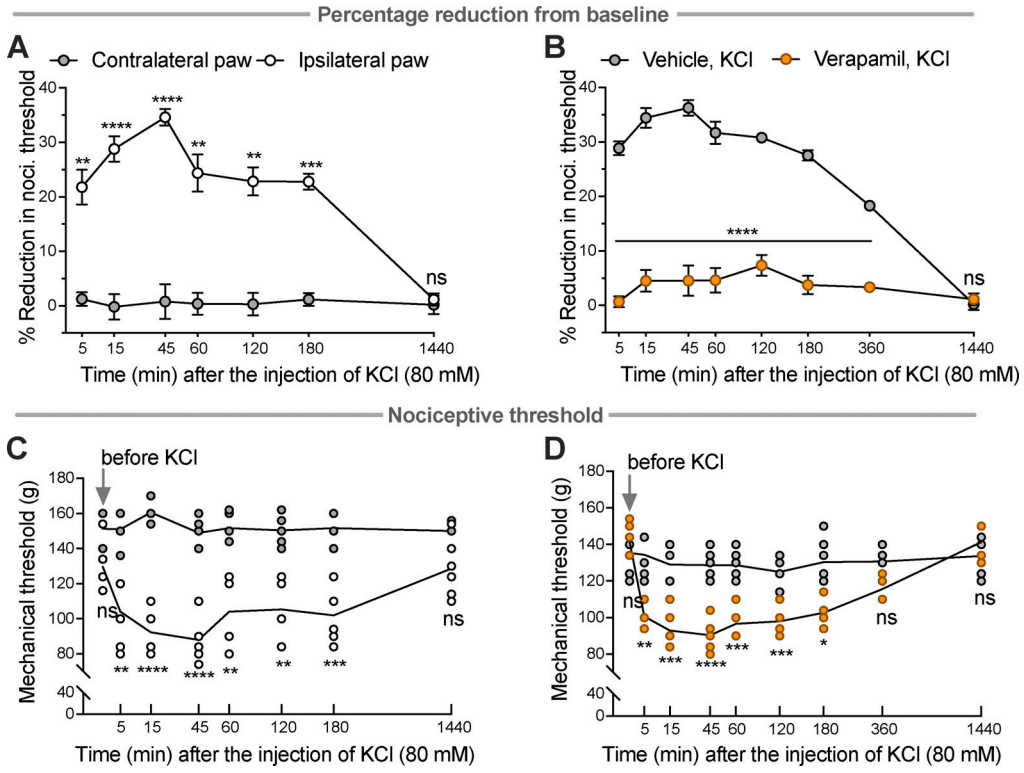

Figure 8. **Depolarization induces hyperalgesia in vivo. (A and C)** Evaluation of mechanical nociceptive thresholds (Randall–Selitto test) 5, 15, 45, 60, 120, 180, and 1,440 min after intradermal injection of KCl (5 µl of 80 mM KCl solution in dH_2O) in the dorsum of the hindpaw of male rats. A biphasic mechanical hyperalgesia was observed in the ipsilateral paw (A, percentage reduction from baseline: $F_{(1,10)}$=186.0, **, P < 0.01, ***, P < 0.001, ****, P < 0.0001; C, nociceptive threshold: $F_{(1,10)}$=47.75, **, P < 0.01, ***, P < 0.001, ****, P < 0.0001, when the ipsilateral and contralateral paws were compared in all time points; two-way repeated-measures ANOVA followed by Sidak's test). **(B and D)** Vehicle (5 µl, dH_2O + 1% ethanol) or verapamil (10 µg diluted in 5 µl dH_2O + 1% ethanol) was injected intradermally in the dorsum of the hindpaw. 30 min later, KCl (5 µl of 80 mM KCl solution in dH_2O) was injected at the same site and mechanical nociceptive threshold evaluated 5, 15, 45, 60, 120, 180, 360, and 1,440 min later. In the group that received verapamil, hyperalgesia was inhibited (B, percentage reduction in nociceptive baseline: $F_{(1,10)}$ = 222.0, ****, P < 0.0001; D, nociceptive threshold: $F_{(1,10)}$ = 22.38, *, P = 0.02, **, P < 0.01, ***, P < 0.001, ****, P < 0.0001, when the vehicle- and verapamil-treated groups are compared at all time points after the injection of KCl; two-way repeated-measures ANOVA followed by Sidak's test). Data represent means ± SEM, *n* = 6 rats per group.

mechanical hyperalgesia in awake behaving animals. We will discuss these aspects in the following sections.

$Ca_V1.2$-dependent induction of intracellular signaling

At synapses, activity-driven changes depend on calcium entry through NMDA/AMPA receptors (Kandel, 2001; Korte and Schmitz, 2016). In primary nociceptive neurons, depolarization-induced calcium currents rely mostly on N-, P/Q-, and T-type channels, while a role for L-type channels such as $Ca_V1.2$ is still considered enigmatic (Bourinet et al., 2014). In the central nervous system, Ca_V1 channels were found to be important in a number of pain conditions. $Ca_V1.2$, localized in spinal dorsal horn neurons, contributes to neuropathy-associated mechanical hypersensitivity (Favereaux et al., 2011; Fossat et al., 2010; Radwani et al., 2016), whereas $Ca_V1.3$ controls the onset of wind-up, a form of short-term central sensitization induced by repetitive noxious stimulation (Favereaux et al., 2011; Fossat et al., 2010; Radwani et al., 2016). In addition, broad-spectrum dihydropyridine inhibitors of $Ca_V1.2$ liter- and $Ca_V3.2$ T-type calcium channels have, although reduced, analgesic effects in $Ca_V3.2$ knockout mice (Gadotti et al., 2015). Expanding this, we now describe a role for $Ca_V1.2$ in depolarization-induced sensitization in the peripheral nociceptive neuron.

Our findings indicate that activation of PKA-II by depolarization requires calcium in $Ca_V1.2$ nanodomains (Tadross et al., 2013), but not bulk cytoplasmic calcium e.g., entering through ionomycin pores. As BAPTA-AM only reduces activation at later time points, close proximity to the channel appears to be important for PKA activation. Indeed, PKA as well as the Ca^{2+}/CaM-activated phosphatase calcineurin (PP2B) are localized to $Ca_V1.2$ by the anchor protein AKAP5 in neurons and myocytes (Dittmer et al., 2014; Hall et al., 2007; Hulme et al., 2003; Murphy et al., 2014; Oliveria et al., 2007; Oliveria et al., 2012; Zhang et al., 2013). In sensory neurons, super-resolution imaging recently revealed that $Ca_V1.2$ channels form multi-channel super-complexes with AKAP5 linking to GPCRs, ACs, and other signaling proteins and thereby enabling local signal transduction in nanodomains (Zhang et al., 2016). Interestingly, though, and in contrast to the GPCR-mediated response to 5-HT, inhibition of Ca^{2+}/CaM-stimulated ACs such as AC1, AC3, and AC8 resulted in local cAMP formation but failed to modulate the induction of PKA-II activity by depolarization (Fig. S4). Also in sharp contrast to 5-HT responses, stimulation of inhibitory GPCRs with opioids or cAMP antagonists were ineffective to block depolarization-induced PKA-II activity indicating distinct mechanisms for

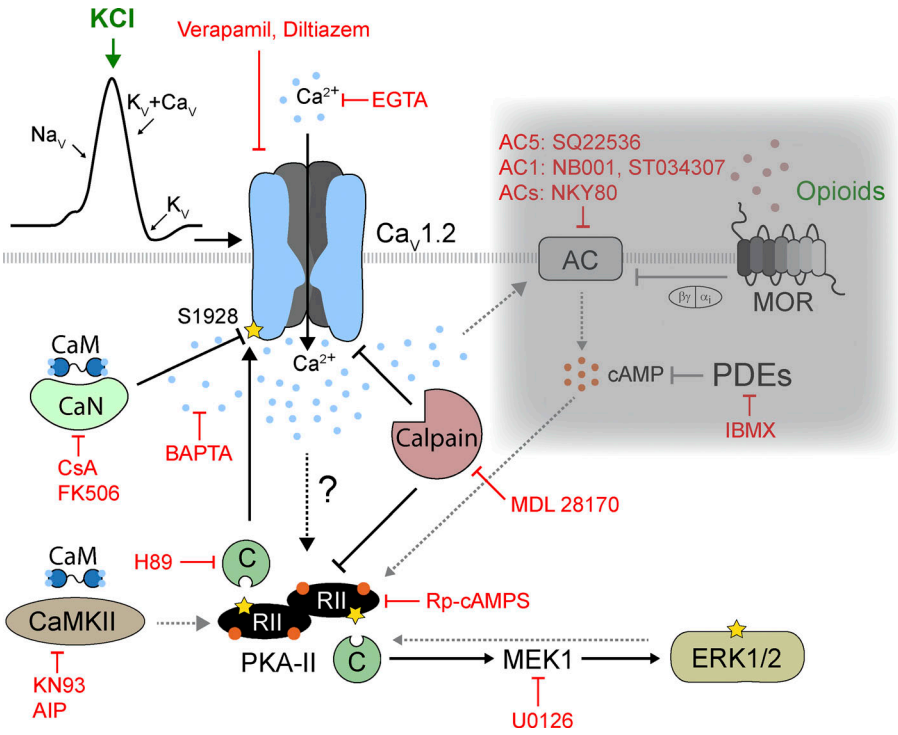

Figure 9. **Model of $Ca_V1.2$ regulation in DRG neurons.** Depolarization of DRG neurons results in $Ca_V1.2$ and calcium-dependent activation of PKA-II. The induction of PKA-II activity is not sensitive to opioids or inhibitors of calcium-stimulated ACs, phosphodiesterases (PDEs), and cAMP antagonists such as Rp-cAMPS, indicating a cAMP-independent activation mechanism (red shadow). In addition, inhibition of CaMKII or ERK1/2 is not affecting the induction of PKA-II activity after depolarization, excluding that PKA-II is downstream of these kinases. Depolarization sensitizes $Ca_V1.2$ by PKA-dependent phosphorylation of Ser1928. Dephosphorylation of $Ca_V1.2$ by the phosphatase calcineurin (CaN) inactivates the channel. CsA, cyclosporine A; MOR, μ opioid receptor.

depolarization- and GPCR-mediated PKA-II activation (Fig. 5). This is in line with many neuropathic pain conditions, which are frequently unresponsive to opioids (Reinecke et al., 2015; Voscopoulos and Lema, 2010).

We tested the hypothesis that calcium-activated calpains digest PKA-RII subunits leading to PKA-II activation (Shell and Lawrence, 2012). Of note, calpain 11 was the only gene upregulated in common in three pain-relevant brain regions after spared-nerve ligation (Descalzi et al., 2017). In the spinal cord, inhibition of calpain has been shown to reduce sciatic nerve ligation induced neuropathic pain (Zhou et al., 2012), lysophosphatidic acid–induced neuropathic pain (Xie et al., 2010) and inflammation-induced thermal hyperalgesia (Kunz et al., 2004). Also in our experiments, the calpain inhibitor MDL 28170 inhibited PKA-II activation after KCl depolarization (Fig. 5 F). This observation potentially links the in vivo effect of MDL 28170 on neuropathic pain to a cellular mechanism, which may be relevant in many neuronal cell types along the pain pathway. MDL 28170, however, did not entirely inhibit PKA-II activation, even at high doses, supporting a modulatory role. The C-terminal domain of $Ca_V1.2$ is proteolytically processed in vivo (De Jongh et al., 1996; Hell et al., 1996), resulting in a cleaved distal C terminus, which inhibits channel activity under basal conditions (Fuller et al., 2010; Hulme et al., 2006b; Wei et al., 1994). Of note, in heterologous expression systems, reconstitution of the PKA-dependent increase in $Ca_V1.2$ current required the presence of both truncated $\alpha_1$1.2 and the separate distal C terminus (Fuller et al., 2010). Therefore, inhibition of proteolysis by MDL 28170 may reduce PKA-dependent channel facilitation, which could also explain why we observed reduced PKA-II activity in the presence of MDL 28170. In addition, calpains cleave the pore-forming $\alpha_1$1.2 subunit of activated $Ca_v1.2$, causing attenuation and biophysical alterations of VGCC currents (Michailidis et al., 2014). This so-called mid-channel proteolysis represents a negative-feedback mechanism reducing calcium influx after longer depolarizations. This may be ruled out, as MDL 28170 should then increase CaV1.2-dependent PKA-II activation, in contrast to the observed decrease.

Our data are driven by pharmacological intervention. The advantage of this is the possibility to corroborate specificity by dose–response experiments as well as the use of structurally unrelated compounds. Further, the fast application route diminishes secondary regulatory effects such as transcriptional/translational changes. Genetic targeting addresses single components and thus is considered to be highly selective. Nevertheless, results are often masked by compensatory counter-regulation of other transcripts, which may reduce the effect size. To corroborate our pharmacological approach, we produced cKO mice lacking $Ca_V1.2$ in $Na_V1.8^+$ nociceptors (Fig. 3). Indeed, the role of $Ca_V1.2$ in regulation of PKA-II was confirmed. However, the effect of the conditional knockout on the KCl dose–response was limited (Fig. 3 H). Counterbalancing expression of $Ca_V2.1$ and 2 as well as $Ca_V3.2$ may not underlie this effect (Fig. 2, A and B), as inhibitors of these channel were ineffective (Fig. 2 C). In contrast to $Ca_V1.2$, these VGCCs (especially $Ca_V3.2$) are also expressed in NF200-expressing DRG neurons, which showed very little activation of PKA-II upon depolarization (Fig. S1 B). Thus, compensation by upregulation of $Ca_V1.3$ (Xu et al., 2003) or ineffective Cre recombination (Harno et al., 2013) may have reduced the effect in cKO mice. This is in line with virus-transduced adult DRG neurons using a *Cacna1c*-specific shRNA to knock down $Ca_V1.2$ (Fig. 4). In agreement with ever-larger reductions of $Ca_V1.2$ over time, we observed a progressive reduction in the basal and induced PKA-II

activity supporting an important, but not necessarily exclusive, role of $Ca_V1.2$ for depolarization-induced activation of PKA-II.

PKA-mediated regulation of calcium channel activity

Intriguingly, blocking the kinase activity of the catalytic subunit of PKA with H89 reduced the pRII response to depolarization (Fig. 6, J and K). This is in contrast to effects of cAMP agonists, which are insensitive to ATP-site inhibitors, because the pRII readout indicates PKA-II dissociation upstream of PKA-II catalytic activity (Isensee et al., 2018). The effect of H89 on depolarization-induced PKA-II activity therefore suggests that PKA-II itself increases $Ca_V1.2$ activity. Indeed, PKA-dependent Ser1928 phosphorylation was shown to enhance neuronal L-type currents (De Jongh et al., 1996; Gao et al., 1997; Hall et al., 2007; Hofmann et al., 2014; Hulme et al., 2006a; Kamp and Hell, 2000; Mitterdorfer et al., 1996; Patriarchi et al., 2016; Weiss et al., 2013) but also primes the channel for Ca^{2+}-dependent inactivation involving calcineurin (Dittmer et al., 2014). In line with this, depolarization of sensory neurons led to transient Ser1928 phosphorylation similar to the PKA-II response and sensitive to $Ca_V1.2$ and PKA inhibitors (Fig. 5, D and H). Consistent with a model in which PKA-dependent phosphorylation of Ser1928 enhances $Ca_V1.2$ gating, inhibition of PKA with H89 partially inhibited ERK1/2 (Fig. 5 L). Further supporting this model, inhibition of calcineurin increased Ser1928 phosphorylation of $Ca_V1.2$ (Fig. 6 I). Following depolarization, $pCa_V1.2$ signals increased in the cytoplasm and slightly delayed also in the nucleus (Fig. 6, F and G). This is in line with a sequential order of phosphorylation-dependent proteolysis and transport. These findings, however, are in contrast to reports using cortical neurons, in which depolarization led to the export of the $Ca_V1.2$ C terminus out of the nucleus, whereas chelating extracellular calcium resulted in nuclear accumulation (Gomez-Ospina et al., 2006). What mechanism underlies this difference and to what extend this is a cell type–specific event will require further studies.

PKA-dependent sensitization toward nociceptive input

PKA is one of the best-established intracellular mediators of pain (Ferreira et al., 1990; Ferreira and Nakamura, 1979; Taiwo et al., 1989). Finding VGCCs to be up- as well as downstream of PKA-II in nociceptors adds a new component to the regulatory network controlled by pro-nociceptive PKA. Ion channels such as $Na_V1.8$ and TRPV1 are well-established targets of PKA downstream of GPCR signaling (Bhave et al., 2002; England et al., 1996; Fitzgerald et al., 1999; Jeske et al., 2008; Rathee et al., 2002; Wang et al., 2007; Zhang et al., 2008). We performed whole-cell patch-clamp electrophysiological recordings before and after applying a train of depolarizations and confirmed that electrical activity results in calcium- and PKA-dependent sensitization of calcium channels in sensory neurons (Fig. 7). This suggests a feed-forward mechanism in which electrical activity sensitizes the nociceptor toward subsequent noxious events. To verify that this concept holds true also in peripheral nociceptive terminals, we measured mechanical pain behavior after KCl injection into the paw. Depolarization of nerve terminals led to transient but rather long-lasting hyperalgesia (Fig. 8 A). Supporting the cellular data, KCl-induced hyperalgesia was sensitive to the same L-type VGCC inhibitor (Fig. 8 B).

In conclusion, our study demonstrates that strong depolarization drives sensitization signaling and hyperalgesia. This supports a novel mechanism regulating the sensitivity of primary afferent neurons specifically after substantial depolarization events. The identified feed-forward mechanism of electrical activity-driven sensitization, which in turn facilitates further electrical activation, opens the possibility of a self-maintaining hyperalgesic state. This is of especial interest, as the identified mechanism is opioid unresponsive, similar to many neuropathic pain states. It will be of great interest to test how this novel mechanism behaves in the plethora of described stimulation paradigms affecting naive as well as diseased sensory neurons.

Materials and methods

Antibodies

The following antibodies were used in this study: chicken polyclonal anti-UCHL1 (1:2,000; Novus; #NB110-58872), rabbit monoclonal anti-RIIα (phospho-Ser96; 1:1,000, clone 151; Abcam; #ab32390), mouse monoclonal anti-RIIβ (1:2,000; BD Transduction Laboratories; #610625), mouse monoclonal anti-NF200 (1:1,000, clone N52; Sigma; #N0142), mouse monoclonal IgG2a anti-CGRP (1:500, clone 4901; Biorbyt/Biozol; #orb319478), mouse monoclonal anti-NaV1.8 (1:500; NeuroMab; clone N134/12, #75-166), rabbit polyclonal anti-$Ca_V1.2$ (phosphor-Ser1928; 1:1,000; Covalab; #pab0692), mouse monoclonal anti-Ca_V1 (1:100, clone L57/46; NeuroMab; catalog no. 75–053), mouse monoclonal anti-$Ca_V1.2$ (1:100, clone N263/31; NeuroMab; catalog no. 73–257), highly cross-adsorbed Alexa Fluor 647–, 555–, and 488–conjugated secondary antibodies (Invitrogen).

Reagents

Diltiazem-HCl (100 mM in distilled H_2O [dH_2O]), D-AP5 (50 mM in dH_2O), lidocaine (100 mM in DMSO), (S)-(-)-Bay K 8644 (50 mM in DMSO), TTA-P2 (10 mM in DMSO), verapamil-HCl (100 mM in dH_2O), ω-conotoxin GVIA (1 mM in dH_2O), ω-conotoxin MVIIC (300 µM in dH_2O), and ω-agatoxin IV A (200 µM in dH_2O) were from Alomone Laboratories and dissolved as indicated in parentheses. AIP (500 µM in dH_2O), H-89 dihydrochloride (10 mM in DMSO), and U0126 (50 mM in DMSO) were from Calbiochem. IBMX (100 mM in DMSO), 5-HT (10 mM in dH_2O), fentanyl (10 mM in dH_2O), NB001 (75 mM in dH_2O), NKY80 (100 mM in DMSO), and oxycodone hydrochloride (10 mM in dH_2O) were from Sigma-Aldrich. FK 506 (50 mM in DMSO), forskolin (10 mM in DMSO), ionomycin calcium salt (10 mM in DMSO), KN-92 (10 mM in DMSO), KN-93 (10 mM in DMSO), [Leu^5]-enkephalin (1 mM in 0.1% BSA in dH_2O), SQ22536 (50 mM in DMSO), and ST 034307 (50 mM in DMSO) were from Tocris. Rp-cAMPS-pAB and 4-ABnOH (10 mM in DMSO) were synthesized and provided by F. Schwede (BioLog, Bremen, Germany).

Animals

For cellular experiments, male Sprague Dawley rats (200–225 g, aged 8–10 wk) were obtained from Harlan. Rats were kept in a

temperature- and humidity-controlled animal care facility at the University Hospital of Cologne on a 12-h light/dark cycle and provided with food and water ad libitum. Male TRPA1 (Kwan et al., 2006), TRPV1 (Caterina et al., 2000), and TRPA1/V1 double-knockout mice (aged 8–12 wk) were provided by John N. Wood (Wolfson Institute for Biomedical Research, University College London, London, UK) and kept on a 12-h light/dark cycle and provided with food and water ad libitum. Conditional $Ca_V1.2$ knockout mice were produced by crossing heterozygous $Na_V1.8$-Cre knock-in mice (Agarwal et al., 2004) provided by Rohini Kuner (Pharmacology Institute, Medical Faculty Heidelberg, Germany) with homozygous floxed $Ca_V1.2$ mice (Seisenberger et al., 2000; Cacna1c^{tm3Hfm}, JAX No. 024714). Offspring were kept on a 12-h light/dark cycle and provided with food and water ad libitum. For cellular experiments, animals were sacrificed between 9 and 12 a.m. by CO_2 intoxication. DRGs (cervical, lumbar, and thoracic) were removed within 30 min per animal. Nociceptive testing was performed on 240–340 g adult male Sprague Dawley rats (Charles River Laboratories). Animals were housed three per cage under a 12-h light/dark cycle in a temperature- and humidity-controlled animal care facility at the University of California, San Francisco. Food and water were available ad libitum. Nociceptive testing was performed between 9:00 a.m. and 5:00 p.m. Experimental protocols were approved by the Institutional Animal Care and Use Committee at the University of California, San Francisco and adhered to the National Institutes of Health Guide for the Care and Use of Laboratory Animals. Effort was made to minimize the number of animals used and their suffering.

AAVs (AAV-PHP.S)

A dual-promoter shRNA rAAV cis vector was used to generate AAV-PHP.S (Chan et al., 2017) expressing *Cacna1c*-specific or scrambled control shRNA driven by an U6 promoter as well as EGFP driven by a CAG promoter (U6-shRNA-CAG-eGFP). The subcloned shRNA sequences were as follows Cacna1c, 5′-TGG AAAGCTCTATACCTGTT-TTCAAGAGAAACAGGTATAGAGCT TTCCTTTTTT-3′; scrambled, 5′-TGGCGCGTATAGTCGCGCGTA TGTCTTCAAGAGAGACATACGCGCGACTATACGCGCC-TTTTTT-3′. These published sequences were validated in hippocampal HT22 cells (Michels et al., 2018). Subcloning of shRNAs and production of viruses was performed by SignaGen Laboratories.

DRG neuron cultures

DRGs were de-sheathed, pooled, and incubated in Neurobasal A/B27 medium (Invitrogen) containing collagenase P (Roche; 0.2 U/ml, 1 h, 37°C, 5% CO_2). DRGs were dissociated by trituration with fire-polished Pasteur pipettes. Axon stumps and disrupted cells were removed by BSA gradient centrifugation (15% BSA, 120 *g*, 8 min). Viable cells were resuspended in Neurobasal A/B27 medium, plated in 0.1 mg/ml poly-L-ornithine/5 µg/ml laminin–precoated 96-well imaging plates (Greiner), and incubated overnight (37°C, 5% CO_2). Neuron density was 1,500 neurons/cm^2.

Stimulation of DRG neurons

DRG neurons were stimulated 24 h after isolation in 96-well imaging plates. Compounds were dissolved in 12.5 µl PBS in 96-well V-bottom plates, mixed with 50 µl medium from the culture wells, and added back to the same wells. Stimulations were performed with automated eight-channel pipettes (Eppendorf) at low dispense speed on heated blocks, and stimulated cells were placed back in the incubator. Kinetic experiments were performed in the reverse order starting with the longest time point. The cells were fixed by adding 100 µl 8% PFA for 10 min at RT, resulting in a final concentration of 4%. When performing experiment with cells from knockout mice, the experimenter was blinded to the genotype.

Immunofluorescence staining

Fixed cells were treated with goat serum blocking (2% goat serum, 1% BSA, 0.1% Triton X-100, and 0.05% Tween 20, 1 h, RT) and incubated with respective primary antibodies diluted in 1% BSA in PBS at 4°C overnight. After three washes with PBS (30 min, RT), cells were incubated with secondary Alexa dye-coupled antibodies (1:1,000, 1 h, RT). After three final washes (30 min, RT), wells of 96-well plates were filled with PBS, sealed, and stored at 4°C until scanning.

Calcium imaging

DRG neurons were seeded in poly-L-ornithine/laminin–precoated 384-well glass-bottom plates (Greiner; #781892) in 100 µl supplemented NB medium and cultured overnight. Then, 70 µl of the medium was removed, 30 µl FLIPR Calcium 5 dye (Molecular Devices; #R8185; dissolved in medium) was added, and the cells were incubated for 1 h in the incubator. Baseline CA5 signal intensities were acquired for 30–60 s with one frame/s, using a Cellomics ArrayScan XTI with LED light source. Images of 1,104 × 1,104 pixels were acquired with a 5× objective (Zeiss). Stimulus was applied fivefold concentrated in 15 µl volume. Images were acquired for 3–5 min with one frame/s. Neurons were depolarized by adding 15 µl 240 mM KCl (final 40 mM) and further imaged for 30 s with one frame/s. The images were analyzed using a customized ImageJ plugin. Raw data were processed with R (R Core Team, 2011).

Quantitative microscopy

We used a Cellomics ArrayScan XTI microscope equipped with an X1 charge-coupled device camera and LED light source to scan stained cultures of DRG neurons in 96-well imaging plates. 2 × 2 binned images (1,104 × 1,104 pixels) were acquired with a 10× (NA = 0.3) EC Plan Neo-Fluor objective (Zeiss) and analyzed using the Cellomics software package. Briefly, images of UCHL1 staining were background corrected (low pass filtration), converted to binary image masks (fixed threshold), and segmented (geometric method), and neurons were identified by the object selection parameters: size of 80–7,500 µm^2, circularity (perimeter^2/4π area) of 1–3, length-to-width ratio of 1–2, average intensity of 800–12,000, and total intensity of 2 × 10^5–5 × 10^7. The image masks were then used to quantify signal in other channels. To calculate spillover between fluorescence channels, three respective controls were prepared for each triple staining: (1) UCHL1 alone, (2) UCHL1 + antibody 1, and (3) UCHL1 + antibody 2. Raw fluorescence data of the controls were used to calculate the slope of best-fit straight lines by linear regression, which

was then used to compensate spillover as described previously (Roederer, 2002). Compensated data were scaled to a mean value of 1 (or 1,000) for the unstimulated cells to adjust for variability between experimental days. 1D and 2D probability density plots were generated using R packages (R Core Team, 2011). Gating of subpopulations was performed by setting thresholds at local minima of probability density plots.

Nociceptive threshold testing

Mechanical nociceptive threshold was measured using an Ugo Basile Analgesymeter (Stoelting; Randall-Selitto paw-withdrawal device), which applies a linearly increasing mechanical force to the dorsum of a rat's hindpaw, with a dome-shaped plinth, as described previously (Araldi et al., 2018). Rats were placed in cylindrical acrylic restrainers that provide ventilation and allow extension of their hind legs from lateral ports to assess nociceptive threshold while minimizing restraint stress. To acclimatize rats to the testing procedure, they were placed in restrainers for 30 min before starting training sessions (three consecutive days of training) and for 30 min before experimental manipulations. Nociceptive threshold was defined as the force, in grams, at which the rat withdrew its paw. Baseline nociceptive threshold was defined as the mean of three readings taken before injection of test agents. Each experiment was performed on a different group of rats and only one paw per rat was used. To minimize experimenter bias, the individual conducting the behavioral experiments (D. Araldi) was blinded to experimental interventions. Intradermal drug administration was performed on the dorsum of the hindpaw using a 30-gauge hypodermic needle adapted to a 50-µl Hamilton syringe by a segment of PE/10 polyethylene tubing (Becton Dickinson). Male rats were treated intradermally with vehicle (5 µl, dH_2O + 1% ethanol) or verapamil (a calcium channel blocker, 10 µg diluted in 5 µl of dH_2O + 1% ethanol). 30 min later, KCl (80 mM diluted in 5 µl dH_2O) was injected intradermally on the dorsum of the hindpaw and mechanical nociceptive threshold evaluated 5, 15, 45, 60, 120, 180, 360, and 1,440 min after its injection. The intradermal administration of vehicle and verapamil were preceded by a hypotonic shock to facilitate the permeability of the cell membrane to these agents (1 µl dH_2O separated by a bubble to avoid mixing in the same syringe) to enhance entry into the nerve terminal (Burch and Axelrod, 1987).

Electrophysiology

The cells kept in 35-mm culture dishes were washed at room temperature (19–23°C) with bath solution immediately before recording. Bath solution contained (in mM) 5 $BaCl_2$ or 5 $CaCl_2$, 1 $MgCl_2$, 10 Hepes, 40 TEA-Cl, and 10 glucose (pH 7.3 with TEA-OH) and the pipette solution (in mM) 110 CsCl, 10 EGTA, 10 Hepes, 5 $MgCl_2$, 4 MgATP, and 0.1 GTP (pH 7.3 with CsOH). For experiments including H89, cells were incubated with 25 µM H89 for 1 h before recording. Holding potential was −90 mV. Patch pipettes made from borosilicate glass (Hilgenberg; 1.7-mm diameter and 0.283-mm wall thickness) were pulled using a Sutter Instrument P-97 horizontal puller and fire-polished using a Narishige MF-83 microforge (Narishige Scientific Instrument Lab). Pipette resistance was 4–6 MΩ. For I-V relation, currents were elicited by applying 500-ms-long test potentials of −40 mV to +60 mV from a holding potential of −90 mV using Clampex software pClamp 10 and an Axopatch 200B amplifier (Molecular Devices). For generation of high Ba^{2+}/Ca^{2+} influx, 1,000-ms-long test potentials to 0 mV were applied (10 times; 0.2 Hz). Holding potential was −90 mV. Currents were sampled at 10 kHz and filtered at 2 kHz. Leak and capacity currents were compensated for. Data were analyzed using pCLAMP10 (Molecular Devices) and GraphPad 6 Prism (GraphPad Software). For voltage dependence of activation, data were fitted by combined Ohm and Boltzmann relation $I(V) = (V - VR) \times \frac{G_{max}}{\left[1+\exp\frac{(V_{0.5}-V)}{dV}\right]}$, according to Karmažínová and Lacinová (2010).

Statistical analysis

Statistical analyses were performed with Student's *t* tests and one- or two-way ANOVA with respective post hoc tests as indicated in the figure legends. $P < 0.05$ was considered statistically significant. Dose–response curves from HCS microscopy were generated using nonlinear regression curve-fitting (three parameters, standard Hill slope) using Prism software (GraphPad). The parameters of the model (top, bottom, or the negative logarithm of the EC_{50}/IC_{50} values) were compared using the extra-sum-of-squares F test. HCS kinetic experiments were analyzed with R (R Core Team, 2011) using ordinary two-way ANOVA. Bonferroni's post hoc analysis was applied to determine P values of selected pairs (i.e., control versus treatment at each time point) defined in a contrast matrix using the R library multcomp. Error bars represent the SEM of three to five independent replicate experiments using cells of different animals. Per experiment, 600–900 neurons were analyzed in one 96-well per condition.

Online supplemental material

Fig. S1 shows a dose–response curve of pRII intensity in mouse DRG neurons exposed to KCl as well as an analysis of neuronal subgroups responding to KCl. Fig. S2 shows the effect of lidocaine on KCl-induced activation of PKA-II, KCl dose–responses in DRG neurons from TRP channel knockout mice, as well as the calcium influx and PKA-II response to ionomycin. Fig. S3 shows immunocytochemistry results of sensory neurons from conditional $Ca_V1.2$ knockout mice and after viral knockdown of $Ca_V1.2$ using a pan-Ca_V1 antibody (clone L57/46). Fig. S4 shows the RNA-seq expression pattern of AC isoforms in rat DRG and the effects of AC inhibitors on KCl-induced PKA-II activity. Fig. S5 shows the effects of CaMKII and MEK inhibitors on KCl-induced PKA-II activity.

Data availability

For material, please contact Jörg Isensee, joerg.isensee@uk-koeln.de, or Tim Hucho, tim.hucho@uk-koeln.de.

Acknowledgments

We thank John N. Wood for providing TRPA1, TRPV1, and TRPA1/V1 double-knockout mice and Maike Siobal and Stephanie Brosig for excellent technical support.

J. Isensee, M. van Cann, and T. Hucho were supported by grants from the German Research Council (grant 3622/0787/11)

and the Federal Ministry of Education and Research (grant 0316177A). K. Moeller was supported by the Evangelisches Studienwerk Villigst and the graduate program in Pharmacology and Experimental Therapeutics at the University of Cologne, which is financially and scientifically supported by Bayer.

The authors declare no competing financial interests.

Author contributions: J. Isensee and T. Hucho designed the study and wrote the manuscript. J. Isensee, M. van Cann, and K. Moeller performed cellular experiments. P. Despang and J. Matthes designed and performed electrophysiological recordings and analyzed data. D. Araldi and J.D. Levine performed mechanical pain testing. J. Petersen and A. Schmidtko contributed to writing the manuscript.

Submitted: 13 February 2020
Revised: 14 June 2021
Accepted: 5 August 2021

References

Agarwal, N., S. Offermanns, and R. Kuner. 2004. Conditional gene deletion in primary nociceptive neurons of trigeminal ganglia and dorsal root ganglia. *Genesis.* 38:122–129. https://doi.org/10.1002/gene.20010

Alexander, S.P., H.E. Benson, E. Faccenda, A.J. Pawson, J.L. Sharman, M. Spedding, J.A. Peters, and A.J. Harmar. CGTP Collaborators. 2013. The Concise Guide to PHARMACOLOGY 2013/14: G protein-coupled receptors. *Br. J. Pharmacol.* 170:1459–1581. https://doi.org/10.1111/bph.12445

Aley, K.O., and J.D. Levine. 1999. Role of protein kinase A in the maintenance of inflammatory pain. *J. Neurosci.* 19:2181–2186. https://doi.org/10.1523/JNEUROSCI.19-06-02181.1999

Araldi, D., E.V. Khomula, L.F. Ferrari, and J.D. Levine. 2018. Fentanyl Induces Rapid Onset Hyperalgesic Priming: Type I at Peripheral and Type II at Central Nociceptor Terminals. *J. Neurosci.* 38:2226–2245. https://doi.org/10.1523/JNEUROSCI.3476-17.2018

Ataman, B., G.L. Boulting, D.A. Harmin, M.G. Yang, M. Baker-Salisbury, E.L. Yap, A.N. Malik, K. Mei, A.A. Rubin, I. Spiegel, et al. 2016. Evolution of Osteocrin as an activity-regulated factor in the primate brain. *Nature.* 539:242–247. https://doi.org/10.1038/nature20111

Bacskai, B.J., B. Hochner, M. Mahaut-Smith, S.R. Adams, B.K. Kaang, E.R. Kandel, and R.Y. Tsien. 1993. Spatially resolved dynamics of cAMP and protein kinase A subunits in Aplysia sensory neurons. *Science.* 260:222–226. https://doi.org/10.1126/science.7682336

Badireddy, S., G. Yunfeng, M. Ritchie, P. Akamine, J. Wu, C.W. Kim, S.S. Taylor, L. Qingsong, K. Swaminathan, and G.S. Anand. 2011. Cyclic AMP analog blocks kinase activation by stabilizing inactive conformation: conformational selection highlights a new concept in allosteric inhibitor design. *Mol. Cell. Proteomics.* 10:M110.004390. https://doi.org/10.1074/mcp.M110.004390

Basbaum, A.I., D.M. Bautista, G. Scherrer, and D. Julius. 2009. Cellular and molecular mechanisms of pain. *Cell.* 139:267–284. https://doi.org/10.1016/j.cell.2009.09.028

Baudry, M., X. Bi, C. Gall, and G. Lynch. 2011. The biochemistry of memory: The 26year journey of a 'new and specific hypothesis'. *Neurobiol. Learn. Mem.* 95:125–133. https://doi.org/10.1016/j.nlm.2010.11.015

Bavencoffe, A., Y. Li, Z. Wu, Q. Yang, J. Herrera, E.J. Kennedy, E.T. Walters, and C.W. Dessauer. 2016. Persistent Electrical Activity in Primary Nociceptors after Spinal Cord Injury Is Maintained by Scaffolded Adenylyl Cyclase and Protein Kinase A and Is Associated with Altered Adenylyl Cyclase Regulation. *J. Neurosci.* 36:1660–1668. https://doi.org/10.1523/JNEUROSCI.0895-15.2016

Bhave, G., W. Zhu, H. Wang, D.J. Brasier, G.S. Oxford, and R.W. Gereau IV. 2002. cAMP-dependent protein kinase regulates desensitization of the capsaicin receptor (VR1) by direct phosphorylation. *Neuron.* 35:721–731. https://doi.org/10.1016/S0896-6273(02)00802-4

Bourinet, E., C. Altier, M.E. Hildebrand, T. Trang, M.W. Salter, and G.W. Zamponi. 2014. Calcium-permeable ion channels in pain signaling. *Physiol. Rev.* 94:81–140. https://doi.org/10.1152/physrev.00023.2013

Brand, C.S., H.J. Hocker, A.A. Gorfe, C.N. Cavasotto, and C.W. Dessauer. 2013. Isoform selectivity of adenylyl cyclase inhibitors: characterization of known and novel compounds. *J. Pharmacol. Exp. Ther.* 347:265–275. https://doi.org/10.1124/jpet.113.208157

Brennan, J.P., S.C. Bardswell, J.R. Burgoyne, W. Fuller, E. Schröder, R. Wait, S. Begum, J.C. Kentish, and P. Eaton. 2006. Oxidant-induced activation of type I protein kinase A is mediated by RI subunit interprotein disulfide bond formation. *J. Biol. Chem.* 281:21827–21836. https://doi.org/10.1074/jbc.M603952200

Brust, T.F., D. Alongkronrusmee, M. Soto-Velasquez, T.A. Baldwin, Z. Ye, M. Dai, C.W. Dessauer, R.M. van Rijn, and V.J. Watts. 2017. Identification of a selective small-molecule inhibitor of type 1 adenylyl cyclase activity with analgesic properties. *Sci. Signal.* 10:eaah5381. https://doi.org/10.1126/scisignal.aah5381

Burch, R.M., and J. Axelrod. 1987. Dissociation of bradykinin-induced prostaglandin formation from phosphatidylinositol turnover in Swiss 3T3 fibroblasts: evidence for G protein regulation of phospholipase A2. *Proc. Natl. Acad. Sci. USA.* 84:6374–6378. https://doi.org/10.1073/pnas.84.18.6374

Burgoyne, J.R., O. Rudyk, H.J. Cho, O. Prysyazhna, N. Hathaway, A. Weeks, R. Evans, T. Ng, K. Schröder, R.P. Brandes, et al. 2015. Deficient angiogenesis in redox-dead Cys17Ser PKARIα knock-in mice. *Nat. Commun.* 6:7920. https://doi.org/10.1038/ncomms8920

Caterina, M.J., A. Leffler, A.B. Malmberg, W.J. Martin, J. Trafton, K.R. Petersen-Zeitz, M. Koltzenburg, A.I. Basbaum, and D. Julius. 2000. Impaired nociception and pain sensation in mice lacking the capsaicin receptor. *Science.* 288:306–313. https://doi.org/10.1126/science.288.5464.306

Chan, K.Y., M.J. Jang, B.B. Yoo, A. Greenbaum, N. Ravi, W.L. Wu, L. Sánchez-Guardado, C. Lois, S.K. Mazmanian, B.E. Deverman, and V. Gradinaru. 2017. Engineered AAVs for efficient noninvasive gene delivery to the central and peripheral nervous systems. *Nat. Neurosci.* 20:1172–1179. https://doi.org/10.1038/nn.4593

Chen, C., J. Zhang, L. Sun, Y. Zhang, W.B. Gan, P. Tang, and G. Yang. 2019. Long-term imaging of dorsal root ganglia in awake behaving mice. *Nat. Commun.* 10:3087. https://doi.org/10.1038/s41467-019-11158-0

Chepurny, O.G., D. Bertinetti, M. Diskar, C.A. Leech, P. Afshari, T. Tsalkova, X. Cheng, F. Schwede, H.G. Genieser, F.W. Herberg, and G.G. Holz. 2013. Stimulation of proglucagon gene expression by human GPR119 in enteroendocrine L-cell line GLUTag. *Mol. Endocrinol.* 27:1267–1282. https://doi.org/10.1210/me.2013-1029

De Jongh, K.S., B.J. Murphy, A.A. Colvin, J.W. Hell, M. Takahashi, and W.A. Catterall. 1996. Specific phosphorylation of a site in the full-length form of the alpha 1 subunit of the cardiac L-type calcium channel by adenosine 3′,5′-cyclic monophosphate-dependent protein kinase. *Biochemistry.* 35:10392–10402. https://doi.org/10.1021/bi953023c

Descalzi, G., V. Mitsi, I. Purushothaman, S. Gaspari, K. Avrampou, Y.E. Loh, L. Shen, and V. Zachariou. 2017. Neuropathic pain promotes adaptive changes in gene expression in brain networks involved in stress and depression. *Sci. Signal.* 10:eaaj1549. https://doi.org/10.1126/scisignal.aaj1549

Dittmer, P.J., M.L. Dell'Acqua, and W.A. Sather. 2014. Ca2+/calcineurin-dependent inactivation of neuronal L-type Ca2+ channels requires priming by AKAP-anchored protein kinase A. *Cell Rep.* 7:1410–1416. https://doi.org/10.1016/j.celrep.2014.04.039

Dolmetsch, R.E., U. Pajvani, K. Fife, J.M. Spotts, and M.E. Greenberg. 2001. Signaling to the nucleus by an L-type calcium channel-calmodulin complex through the MAP kinase pathway. *Science.* 294:333–339. https://doi.org/10.1126/science.1063395

Dolphin, A.C. 1991. Ca2+ channel currents in rat sensory neurones: interaction between guanine nucleotides, cyclic AMP and Ca2+ channel ligands. *J. Physiol.* 432:23–43. https://doi.org/10.1113/jphysiol.1991.sp018374

Dulin, N.O., J. Niu, D.D. Browning, R.D. Ye, and T. Voyno-Yasenetskaya. 2001. Cyclic AMP-independent activation of protein kinase A by vasoactive peptides. *J. Biol. Chem.* 276:20827–20830. https://doi.org/10.1074/jbc.C100195200

England, S., S. Bevan, and R.J. Docherty. 1996. PGE2 modulates the tetrodotoxin-resistant sodium current in neonatal rat dorsal root ganglion neurones via the cyclic AMP-protein kinase A cascade. *J. Physiol.* 495:429–440. https://doi.org/10.1113/jphysiol.1996.sp021604

Favereaux, A., O. Thoumine, R. Bouali-Benazzouz, V. Roques, M.A. Papon, S.A. Salam, G. Drutel, C. Léger, A. Calas, F. Nagy, and M. Landry. 2011. Bidirectional integrative regulation of Cav1.2 calcium channel by microRNA miR-103: role in pain. *EMBO J.* 30:3830–3841. https://doi.org/10.1038/emboj.2011.249

Ferreira, S.H., and M. Nakamura. 1979. I - Prostaglandin hyperalgesia, a cAMP/Ca2+ dependent process. *Prostaglandins.* 18:179–190. https://doi.org/10.1016/0090-6980(79)90103-5

Ferreira, S.H., B.B. Lorenzetti, and D.I. De Campos. 1990. Induction, blockade and restoration of a persistent hypersensitive state. *Pain.* 42:365–371. https://doi.org/10.1016/0304-3959(90)91149-D

Fitzgerald, E.M., K. Okuse, J.N. Wood, A.C. Dolphin, and S.J. Moss. 1999. cAMP-dependent phosphorylation of the tetrodotoxin-resistant voltage-dependent sodium channel SNS. *J. Physiol.* 516:433–446. https://doi.org/10.1111/j.1469-7793.1999.0433v.x

Fossat, P., E. Dobremez, R. Bouali-Benazzouz, A. Favereaux, S.S. Bertrand, K. Kilk, C. Léger, J.R. Cazalets, U. Langel, M. Landry, and F. Nagy. 2010. Knockdown of L calcium channel subtypes: differential effects in neuropathic pain. *J. Neurosci.* 30:1073–1085. https://doi.org/10.1523/JNEUROSCI.3145-09.2010

Fuller, M.D., M.A. Emrick, M. Sadilek, T. Scheuer, and W.A. Catterall. 2010. Molecular mechanism of calcium channel regulation in the fight-or-flight response. *Sci. Signal.* 3:ra70. https://doi.org/10.1126/scisignal.2001152

Gadotti, V.M., C. Bladen, F.X. Zhang, L. Chen, M.G. Gündüz, R. Şimşek, C. Şafak, and G.W. Zamponi. 2015. Analgesic effect of a broad-spectrum dihydropyridine inhibitor of voltage-gated calcium channels. *Pflugers Arch.* 467:2485–2493. https://doi.org/10.1007/s00424-015-1725-1

Gao, T., A. Yatani, M.L. Dell'Acqua, H. Sako, S.A. Green, N. Dascal, J.D. Scott, and M.M. Hosey. 1997. cAMP-dependent regulation of cardiac L-type Ca2+ channels requires membrane targeting of PKA and phosphorylation of channel subunits. *Neuron.* 19:185–196. https://doi.org/10.1016/S0896-6273(00)80358-X

Gao, L., L.A. Blair, and J. Marshall. 2006. CaMKII-independent effects of KN93 and its inactive analog KN92: reversible inhibition of L-type calcium channels. *Biochem. Biophys. Res. Commun.* 345:1606–1610. https://doi.org/10.1016/j.bbrc.2006.05.066

Gjertsen, B.T., G. Mellgren, A. Otten, E. Maronde, H.G. Genieser, B. Jastorff, O.K. Vintermyr, G.S. McKnight, and S.O. Døskeland. 1995. Novel (Rp)-cAMPS analogs as tools for inhibition of cAMP-kinase in cell culture. Basal cAMP-kinase activity modulates interleukin-1 beta action. *J. Biol. Chem.* 270:20599–20607. https://doi.org/10.1074/jbc.270.35.20599

Gomez-Ospina, N., F. Tsuruta, O. Barreto-Chang, L. Hu, and R. Dolmetsch. 2006. The C terminus of the L-type voltage-gated calcium channel Ca(V)1.2 encodes a transcription factor. *Cell.* 127:591–606. https://doi.org/10.1016/j.cell.2006.10.017

Greengard, P. 2001. The neurobiology of slow synaptic transmission. *Science.* 294:1024–1030. https://doi.org/10.1126/science.294.5544.1024

Greer, P.L., and M.E. Greenberg. 2008. From synapse to nucleus: calcium-dependent gene transcription in the control of synapse development and function. *Neuron.* 59:846–860. https://doi.org/10.1016/j.neuron.2008.09.002

Hall, D.D., M.A. Davare, M. Shi, M.L. Allen, M. Weisenhaus, G.S. McKnight, and J.W. Hell. 2007. Critical role of cAMP-dependent protein kinase anchoring to the L-type calcium channel Cav1.2 via A-kinase anchor protein 150 in neurons. *Biochemistry.* 46:1635–1646. https://doi.org/10.1021/bi062217x

Harno, E., E.C. Cottrell, and A. White. 2013. Metabolic pitfalls of CNS Cre-based technology. *Cell Metab.* 18:21–28. https://doi.org/10.1016/j.cmet.2013.05.019

Hell, J.W., R.E. Westenbroek, L.J. Breeze, K.K. Wang, C. Chavkin, and W.A. Catterall. 1996. N-methyl-D-aspartate receptor-induced proteolytic conversion of postsynaptic class C L-type calcium channels in hippocampal neurons. *Proc. Natl. Acad. Sci. USA.* 93:3362–3367. https://doi.org/10.1073/pnas.93.8.3362

Henrich, F., W. Magerl, T. Klein, W. Greffrath, and R.D. Treede. 2015. Capsaicin-sensitive C- and A-fibre nociceptors control long-term potentiation-like pain amplification in humans. *Brain.* 138:2505–2520. https://doi.org/10.1093/brain/awv108

Hofmann, F., V. Flockerzi, S. Kahl, and J.W. Wegener. 2014. L-type CaV1.2 calcium channels: from in vitro findings to in vivo function. *Physiol. Rev.* 94:303–326. https://doi.org/10.1152/physrev.00016.2013

Hucho, T., and J.D. Levine. 2007. Signaling pathways in sensitization: toward a nociceptor cell biology. *Neuron.* 55:365–376. https://doi.org/10.1016/j.neuron.2007.07.008

Hulme, J.T., T.W. Lin, R.E. Westenbroek, T. Scheuer, and W.A. Catterall. 2003. Beta-adrenergic regulation requires direct anchoring of PKA to cardiac CaV1.2 channels via a leucine zipper interaction with A kinase-anchoring protein 15. *Proc. Natl. Acad. Sci. USA.* 100:13093–13098. https://doi.org/10.1073/pnas.2135335100

Hulme, J.T., R.E. Westenbroek, T. Scheuer, and W.A. Catterall. 2006a. Phosphorylation of serine 1928 in the distal C-terminal domain of cardiac CaV1.2 channels during beta1-adrenergic regulation. *Proc. Natl. Acad. Sci. USA.* 103:16574–16579. https://doi.org/10.1073/pnas.0607294103

Hulme, J.T., V. Yarov-Yarovoy, T.W. Lin, T. Scheuer, and W.A. Catterall. 2006b. Autoinhibitory control of the CaV1.2 channel by its proteolytically processed distal C-terminal domain. *J. Physiol.* 576:87–102. https://doi.org/10.1113/jphysiol.2006.111799

Impey, S., K. Obrietan, S.T. Wong, S. Poser, S. Yano, G. Wayman, J.C. Deloulme, G. Chan, and D.R. Storm. 1998. Cross talk between ERK and PKA is required for Ca2+ stimulation of CREB-dependent transcription and ERK nuclear translocation. *Neuron.* 21:869–883. https://doi.org/10.1016/S0896-6273(00)80602-9

Isensee, J., and T. Hucho. 2019. High-Content Imaging of Immunofluorescently Labeled TRPV1-Positive Sensory Neurons. *Methods Mol. Biol.* 1987:111–124. https://doi.org/10.1007/978-1-4939-9446-5_8

Isensee, J., M. Diskar, S. Waldherr, R. Buschow, J. Hasenauer, A. Prinz, F. Allgöwer, F.W. Herberg, and T. Hucho. 2014a. Pain modulators regulate the dynamics of PKA-RII phosphorylation in subgroups of sensory neurons. *J. Cell Sci.* 127:216–229. https://doi.org/10.1242/jcs.136580

Isensee, J., C. Wenzel, R. Buschow, R. Weissmann, A.W. Kuss, and T. Hucho. 2014b. Subgroup-elimination transcriptomics identifies signaling proteins that define subclasses of TRPV1-positive neurons and a novel paracrine circuit. *PLoS One.* 9:e115731. https://doi.org/10.1371/journal.pone.0115731

Isensee, J., L. Krahé, K. Moeller, V. Pereira, J.E. Sexton, X. Sun, E. Emery, J.N. Wood, and T. Hucho. 2017a. Synergistic regulation of serotonin and opioid signaling contributes to pain insensitivity in Nav1.7 knockout mice. *Sci. Signal.* 10:eaah4874. https://doi.org/10.1126/scisignal.aah4874

Isensee, J., C. Schild, F. Schwede, and T. Hucho. 2017b. Crosstalk from cAMP to ERK1/2 emerges during postnatal maturation of nociceptive neurons and is maintained during aging. *J. Cell Sci.* 130:2134–2146.

Isensee, J., M. Kaufholz, M.J. Knape, J. Hasenauer, H. Hammerich, H. Gonczarowska-Jorge, R.P. Zahedi, F. Schwede, F.W. Herberg, and T. Hucho. 2018. PKA-RII subunit phosphorylation precedes activation by cAMP and regulates activity termination. *J. Cell Biol.* 217:2167–2184. https://doi.org/10.1083/jcb.201708053

Jeske, N.A., A. Diogenes, N.B. Ruparel, J.C. Fehrenbacher, M. Henry, A.N. Akopian, and K.M. Hargreaves. 2008. A-kinase anchoring protein mediates TRPV1 thermal hyperalgesia through PKA phosphorylation of TRPV1. *Pain.* 138:604–616. https://doi.org/10.1016/j.pain.2008.02.022

Kamp, T.J., and J.W. Hell. 2000. Regulation of cardiac L-type calcium channels by protein kinase A and protein kinase C. *Circ. Res.* 87:1095–1102. https://doi.org/10.1161/01.RES.87.12.1095

Kandel, E.R. 2001. The molecular biology of memory storage: a dialogue between genes and synapses. *Science.* 294:1030–1038. https://doi.org/10.1126/science.1067020

Karmažínová, M., and L. Lacinová. 2010. Measurement of cellular excitability by whole cell patch clamp technique. *Physiol. Res.* 59(Suppl 1):S1–S7. https://doi.org/10.33549/physiolres.932000

Kim, K.S., K.W. Lee, K.W. Lee, J.Y. Im, J.Y. Yoo, S.W. Kim, J.K. Lee, E.J. Nestler, and P.L. Han. 2006. Adenylyl cyclase type 5 (AC5) is an essential mediator of morphine action. *Proc. Natl. Acad. Sci. USA.* 103:3908–3913. https://doi.org/10.1073/pnas.0508812103

Kim, K.S., J. Kim, S.K. Back, J.Y. Im, H.S. Na, and P.L. Han. 2007. Markedly attenuated acute and chronic pain responses in mice lacking adenylyl cyclase-5. *Genes Brain Behav.* 6:120–127. https://doi.org/10.1111/j.1601-183X.2006.00238.x

Kim, T.K., M. Hemberg, J.M. Gray, A.M. Costa, D.M. Bear, J. Wu, D.A. Harmin, M. Laptewicz, K. Barbara-Haley, S. Kuersten, et al. 2010. Widespread transcription at neuronal activity-regulated enhancers. *Nature.* 465:182–187. https://doi.org/10.1038/nature09033

Korte, M., and D. Schmitz. 2016. Cellular and System Biology of Memory: Timing, Molecules, and Beyond. *Physiol. Rev.* 96:647–693. https://doi.org/10.1152/physrev.00010.2015

Kuner, R., and H. Flor. 2016. Structural plasticity and reorganisation in chronic pain. *Nat. Rev. Neurosci.* 18:20–30. https://doi.org/10.1038/nrn.2016.162

Kunz, S., E. Niederberger, C. Ehnert, O. Coste, A. Pfenninger, J. Kruip, T.M. Wendrich, A. Schmidtko, I. Tegeder, and G. Geisslinger. 2004. The calpain inhibitor MDL 28170 prevents inflammation-induced neurofilament light chain breakdown in the spinal cord and reduces thermal hyperalgesia. *Pain.* 110:409–418. https://doi.org/10.1016/j.pain.2004.04.031

Kwan, K.Y., A.J. Allchorne, M.A. Vollrath, A.P. Christensen, D.S. Zhang, C.J. Woolf, and D.P. Corey. 2006. TRPA1 contributes to cold, mechanical, and chemical nociception but is not essential for hair-cell transduction. *Neuron.* 50:277–289. https://doi.org/10.1016/j.neuron.2006.03.042

Latremoliere, A., and C.J. Woolf. 2009. Central sensitization: a generator of pain hypersensitivity by central neural plasticity. *J. Pain.* 10:895–926. https://doi.org/10.1016/j.jpain.2009.06.012

Liao, X., J.D. Gunstream, M.R. Lewin, R.T. Ambron, and E.T. Walters. 1999. Activation of protein kinase A contributes to the expression but not the induction of long-term hyperexcitability caused by axotomy of Aplysia sensory neurons. *J. Neurosci.* 19:1247–1256. https://doi.org/10.1523/JNEUROSCI.19-04-01247.1999

Ma, H., R.D. Groth, S.M. Cohen, J.F. Emery, B. Li, E. Hoedt, G. Zhang, T.A. Neubert, and R.W. Tsien. 2014. γCaMKII shuttles Ca^{2+}/CaM to the nucleus to trigger CREB phosphorylation and gene expression. *Cell.* 159: 281–294. https://doi.org/10.1016/j.cell.2014.09.019

Malik, Z.A., I.S. Stein, M.F. Navedo, and J.W. Hell. 2014. Mission CaMKIIγ: shuttle calmodulin from membrane to nucleus. *Cell.* 159:235–237. https://doi.org/10.1016/j.cell.2014.09.023

Michailidis, I.E., K. Abele-Henckels, W.K. Zhang, B. Lin, Y. Yu, L.S. Geyman, M.D. Ehlers, E.A. Pnevmatikakis, and J. Yang. 2014. Age-related homeostatic midchannel proteolysis of neuronal L-type voltage-gated Ca^{2+} channels. *Neuron.* 82:1045–1057. https://doi.org/10.1016/j.neuron.2014.04.017

Michels, S., G.K. Ganjam, H. Martins, G.M. Schratt, M. Wöhr, R.K.W. Schwarting, and C. Culmsee. 2018. Downregulation of the psychiatric susceptibility gene *Cacna1c* promotes mitochondrial resilience to oxidative stress in neuronal cells. *Cell Death Discov.* 4:54. https://doi.org/10.1038/s41420-018-0061-6

Mitterdorfer, J., M. Froschmayr, M. Grabner, F.F. Moebius, H. Glossmann, and J. Striessnig. 1996. Identification of PK-A phosphorylation sites in the carboxyl terminus of L-type calcium channel alpha 1 subunits. *Biochemistry.* 35:9400–9406. https://doi.org/10.1021/bi960683o

Murphy, J.G., J.L. Sanderson, J.A. Gorski, J.D. Scott, W.A. Catterall, W.A. Sather, and M.L. Dell'Acqua. 2014. AKAP-anchored PKA maintains neuronal L-type calcium channel activity and NFAT transcriptional signaling. *Cell Rep.* 7:1577–1588. https://doi.org/10.1016/j.celrep.2014.04.027

North, R.Y., T.T. Lazaro, and P.M. Dougherty. 2018. Ectopic Spontaneous Afferent Activity and Neuropathic Pain. *Neurosurgery.* 65(CN_suppl_1): 49–54. https://doi.org/10.1093/neuros/nyy119

Oliveria, S.F., M.L. Dell'Acqua, and W.A. Sather. 2007. AKAP79/150 anchoring of calcineurin controls neuronal L-type Ca2+ channel activity and nuclear signaling. *Neuron.* 55:261–275. https://doi.org/10.1016/j.neuron.2007.06.032

Oliveria, S.F., P.J. Dittmer, D.H. Youn, M.L. Dell'Acqua, and W.A. Sather. 2012. Localized calcineurin confers Ca2+-dependent inactivation on neuronal L-type Ca2+ channels. *J. Neurosci.* 32:15328–15337. https://doi.org/10.1523/JNEUROSCI.2302-12.2012

Patriarchi, T., H. Qian, V. Di Biase, Z.A. Malik, D. Chowdhury, J.L. Price, E.A. Hammes, O.R. Buonarati, R.E. Westenbroek, W.A. Catterall, et al. 2016. Phosphorylation of Cav1.2 on S1928 uncouples the L-type Ca2+ channel from the β2 adrenergic receptor. *EMBO J.* 35:1330–1345. https://doi.org/10.15252/embj.201593409

Prinz, A., M. Diskar, A. Erlbruch, and F.W. Herberg. 2006. Novel, isotype-specific sensors for protein kinase A subunit interaction based on bioluminescence resonance energy transfer (BRET). *Cell. Signal.* 18: 1616–1625. https://doi.org/10.1016/j.cellsig.2006.01.013

R Core Team. 2011. R: A Language and Environment for Statistical Computing. R Foundation for Statistical Computing, Vienna, Austria.

Radwani, H., M.J. Lopez-Gonzalez, D. Cattaert, O. Roca-Lapirot, E. Dobremez, R. Bouali-Benazzouz, E. Eiríksdóttir, Ü. Langel, A. Favereaux, M. Errami, et al. 2016. Cav1.2 and Cav1.3 L-type calcium channels independently control short- and long-term sensitization to pain. *J. Physiol.* 594: 6607–6626. https://doi.org/10.1113/JP272725

Rathee, P.K., C. Distler, O. Obreja, W. Neuhuber, G.K. Wang, S.Y. Wang, C. Nau, and M. Kress. 2002. PKA/AKAP/VR-1 module: A common link of Gs-mediated signaling to thermal hyperalgesia. *J. Neurosci.* 22:4740–4745. https://doi.org/10.1523/JNEUROSCI.22-11-04740.2002

Reinecke, H., C. Weber, K. Lange, M. Simon, C. Stein, and H. Sorgatz. 2015. Analgesic efficacy of opioids in chronic pain: recent meta-analyses. *Br. J. Pharmacol.* 172:324–333. https://doi.org/10.1111/bph.12634

Roederer, M. 2002. Compensation in flow cytometry. Curr. Protoc. Cytom. Chapter 1:Unit 1.14.

Rosen, L.B., and M.E. Greenberg. 1996. Stimulation of growth factor receptor signal transduction by activation of voltage-sensitive calcium channels. *Proc. Natl. Acad. Sci. USA.* 93:1113–1118. https://doi.org/10.1073/pnas.93.3.1113

Rosen, L.B., D.D. Ginty, M.J. Weber, and M.E. Greenberg. 1994. Membrane depolarization and calcium influx stimulate MEK and MAP kinase via activation of Ras. *Neuron.* 12:1207–1221. https://doi.org/10.1016/0896-6273(94)90438-3

Rothermel, J.D., W.J. Stec, J. Baraniak, B. Jastorff, and L.H. Botelho. 1983. Inhibition of glycogenolysis in isolated rat hepatocytes by the Rp diastereomer of adenosine cyclic 3′,5′-phosphorothioate. *J. Biol. Chem.* 258: 12125–12128. https://doi.org/10.1016/S0021-9258(17)44142-1

Sandkühler, J. 2009. Models and mechanisms of hyperalgesia and allodynia. *Physiol. Rev.* 89:707–758. https://doi.org/10.1152/physrev.00025.2008

Schwede, F., O.G. Chepurny, M. Kaufholz, D. Bertinetti, C.A. Leech, O. Cabrera, Y. Zhu, F. Mei, X. Cheng, J.E. Manning Fox, et al. 2015. Rp-cAMPS Prodrugs Reveal the cAMP Dependence of First-Phase Glucose-Stimulated Insulin Secretion. *Mol. Endocrinol.* 29:988–1005. https://doi.org/10.1210/me.2014-1330

Seisenberger, C., V. Specht, A. Welling, J. Platzer, A. Pfeifer, S. Kühbandner, J. Striessnig, N. Klugbauer, R. Feil, and F. Hofmann. 2000. Functional embryonic cardiomyocytes after disruption of the L-type alpha1C (Cav1.2) calcium channel gene in the mouse. *J. Biol. Chem.* 275: 39193–39199. https://doi.org/10.1074/jbc.M006467200

Sharif-Naeini, R., and A.I. Basbaum. 2011. Targeting pain where it resides… In the brain. *Sci. Transl. Med.* 3:65ps1. https://doi.org/10.1126/scitranslmed.3002077

Shell, J.R., and D.S. Lawrence. 2012. Proteolytic regulation of the mitochondrial cAMP-dependent protein kinase. *Biochemistry.* 51:2258–2264. https://doi.org/10.1021/bi201573k

Song, X.J., Z.B. Wang, Q. Gan, and E.T. Walters. 2006. cAMP and cGMP contribute to sensory neuron hyperexcitability and hyperalgesia in rats with dorsal root ganglia compression. *J. Neurophysiol.* 95:479–492. https://doi.org/10.1152/jn.00503.2005

Tadross, M.R., R.W. Tsien, and D.T. Yue. 2013. Ca2+ channel nanodomains boost local Ca2+ amplitude. *Proc. Natl. Acad. Sci. USA.* 110:15794–15799. https://doi.org/10.1073/pnas.1313898110

Taiwo, Y.O., L.K. Bjerknes, E.J. Goetzl, and J.D. Levine. 1989. Mediation of primary afferent peripheral hyperalgesia by the cAMP second messenger system. *Neuroscience.* 32:577–580. https://doi.org/10.1016/0306-4522(89)90280-7

Villarreal, C.F., D. Sachs, M.I. Funez, C.A. Parada, F. de Queiroz Cunha, and S.H. Ferreira. 2009. The peripheral pro-nociceptive state induced by repetitive inflammatory stimuli involves continuous activation of protein kinase A and protein kinase C epsilon and its Na(V)1.8 sodium channel functional regulation in the primary sensory neuron. *Biochem. Pharmacol.* 77:867–877. https://doi.org/10.1016/j.bcp.2008.11.015

Voscopoulos, C., and M. Lema. 2010. When does acute pain become chronic? *Br. J. Anaesth.* 105(Suppl 1):i69–i85. https://doi.org/10.1093/bja/aeq323

Wang, C., G.W. Li, and L.Y. Huang. 2007. Prostaglandin E2 potentiation of P2X3 receptor mediated currents in dorsal root ganglion neurons. *Mol. Pain.* 3:22. https://doi.org/10.1186/1744-8069-3-22

Wang, H., H. Xu, L.J. Wu, S.S. Kim, T. Chen, K. Koga, G. Descalzi, B. Gong, K.I. Vadakkan, X. Zhang, et al. 2011. Identification of an adenylyl cyclase inhibitor for treating neuropathic and inflammatory pain. *Sci. Transl. Med.* 3:65ra3. https://doi.org/10.1126/scitranslmed.3001269

Wei, X., A. Neely, A.E. Lacerda, R. Olcese, E. Stefani, E. Perez-Reyes, and L. Birnbaumer. 1994. Modification of Ca2+ channel activity by deletions at the carboxyl terminus of the cardiac alpha 1 subunit. *J. Biol. Chem.* 269: 1635–1640. https://doi.org/10.1016/S0021-9258(17)42074-6

Wei, F., C.S. Qiu, S.J. Kim, L. Muglia, J.W. Maas, V.V. Pineda, H.M. Xu, Z.F. Chen, D.R. Storm, L.J. Muglia, and M. Zhuo. 2002. Genetic elimination of behavioral sensitization in mice lacking calmodulin-stimulated adenylyl cyclases. *Neuron.* 36:713–726. https://doi.org/10.1016/S0896-6273(02)01019-X

Wei, F., K.I. Vadakkan, H. Toyoda, L.J. Wu, M.G. Zhao, H. Xu, F.W. Shum, Y.H. Jia, and M. Zhuo. 2006. Calcium calmodulin-stimulated adenylyl cyclases contribute to activation of extracellular signal-regulated kinase in spinal dorsal horn neurons in adult rats and mice. *J. Neurosci.* 26: 851–861. https://doi.org/10.1523/JNEUROSCI.3292-05.2006

Weiss, S., S. Oz, A. Benmocha, and N. Dascal. 2013. Regulation of cardiac L-type Ca^{2+} channel CaV1.2 via the β-adrenergic-cAMP-protein kinase A pathway: old dogmas, advances, and new uncertainties. *Circ. Res.* 113: 617–631. https://doi.org/10.1161/CIRCRESAHA.113.301781

Wheeler, D.G., C.F. Barrett, R.D. Groth, P. Safa, and R.W. Tsien. 2008. CaMKII locally encodes L-type channel activity to signal to nuclear CREB in excitation-transcription coupling. *J. Cell Biol.* 183:849–863. https://doi.org/10.1083/jcb.200805048

Wheeler, D.G., R.D. Groth, H. Ma, C.F. Barrett, S.F. Owen, P. Safa, and R.W. Tsien. 2012. Ca(V)1 and Ca(V)2 channels engage distinct modes of Ca(2+) signaling to control CREB-dependent gene expression. *Cell.* 149: 1112–1124. https://doi.org/10.1016/j.cell.2012.03.041

Wu, G.Y., K. Deisseroth, and R.W. Tsien. 2001. Activity-dependent CREB phosphorylation: convergence of a fast, sensitive calmodulin kinase pathway and a slow, less sensitive mitogen-activated protein kinase pathway. *Proc. Natl. Acad. Sci. USA.* 98:2808–2813. https://doi.org/10.1073/pnas.051634198

Xie, W., H. Uchida, J. Nagai, M. Ueda, J. Chun, and H. Ueda. 2010. Calpain-mediated down-regulation of myelin-associated glycoprotein in lysophosphatidic acid-induced neuropathic pain. *J. Neurochem.* 113: 1002–1011. https://doi.org/10.1111/j.1471-4159.2010.06664.x

Xu, M., A. Welling, S. Paparisto, F. Hofmann, and N. Klugbauer. 2003. Enhanced expression of L-type Cav1.3 calcium channels in murine embryonic hearts from Cav1.2-deficient mice. *J. Biol. Chem.* 278: 40837–40841. https://doi.org/10.1074/jbc.M307598200

Xu, J., L. Yu, E. Minobe, L. Lu, M. Lei, and M. Kameyama. 2016. PKA and phosphatases attached to the Ca(V)1.2 channel regulate channel activity in cell-free patches. *Am. J. Physiol. Cell Physiol.* 310:C136–C141. https://doi.org/10.1152/ajpcell.00157.2015

Zamponi, G.W. 2016. Targeting voltage-gated calcium channels in neurological and psychiatric diseases. *Nat. Rev. Drug Discov.* 15:19–34. https://doi.org/10.1038/nrd.2015.5

Zamponi, G.W., J. Striessnig, A. Koschak, and A.C. Dolphin. 2015. The Physiology, Pathology, and Pharmacology of Voltage-Gated Calcium Channels and Their Future Therapeutic Potential. *Pharmacol. Rev.* 67: 821–870. https://doi.org/10.1124/pr.114.009654

Zeisel, A., H. Hochgerner, P. Lönnerberg, A. Johnsson, F. Memic, J. van der Zwan, M. Häring, E. Braun, L.E. Borm, G. La Manno, et al. 2018. Molecular Architecture of the Mouse Nervous System. *Cell.* 174:999–1014.e22. https://doi.org/10.1016/j.cell.2018.06.021

Zhang, X., L. Li, and P.A. McNaughton. 2008. Proinflammatory mediators modulate the heat-activated ion channel TRPV1 via the scaffolding protein AKAP79/150. *Neuron.* 59:450–461. https://doi.org/10.1016/j.neuron.2008.05.015

Zhang, P., E.V. Smith-Nguyen, M.M. Keshwani, M.S. Deal, A.P. Kornev, and S.S. Taylor. 2012. Structure and allostery of the PKA RIIβ tetrameric holoenzyme. *Science.* 335:712–716. https://doi.org/10.1126/science.1213979

Zhang, M., T. Patriarchi, I.S. Stein, H. Qian, L. Matt, M. Nguyen, Y.K. Xiang, and J.W. Hell. 2013. Adenylyl cyclase anchoring by a kinase anchor protein AKAP5 (AKAP79/150) is important for postsynaptic β-adrenergic signaling. *J. Biol. Chem.* 288:17918–17931. https://doi.org/10.1074/jbc.M112.449462

Zhang, P., M.J. Knape, L.G. Ahuja, M.M. Keshwani, C.C. King, M. Sastri, F.W. Herberg, and S.S. Taylor. 2015. Single Turnover Autophosphorylation Cycle of the PKA RIIβ Holoenzyme. *PLoS Biol.* 13:e1002192. https://doi.org/10.1371/journal.pbio.1002192

Zhang, J., C.M. Carver, F.S. Choveau, and M.S. Shapiro. 2016. Clustering and Functional Coupling of Diverse Ion Channels and Signaling Proteins Revealed by Super-resolution STORM Microscopy in Neurons. *Neuron.* 92:461–478. https://doi.org/10.1016/j.neuron.2016.09.014

Zhong, H., H. SuYang, H. Erdjument-Bromage, P. Tempst, and S. Ghosh. 1997. The transcriptional activity of NF-kappaB is regulated by the IkappaB-associated PKAc subunit through a cyclic AMP-independent mechanism. *Cell.* 89:413–424. https://doi.org/10.1016/S0092-8674(00)80222-6

Zhou, H.Y., S.R. Chen, H.S. Byun, H. Chen, L. Li, H.D. Han, G. Lopez-Berestein, A.K. Sood, and H.L. Pan. 2012. N-methyl-D-aspartate receptor- and calpain-mediated proteolytic cleavage of K+-Cl- cotransporter-2 impairs spinal chloride homeostasis in neuropathic pain. *J. Biol. Chem.* 287:33853–33864. https://doi.org/10.1074/jbc.M112.395830

Zühlke, R.D., G.S. Pitt, K. Deisseroth, R.W. Tsien, and H. Reuter. 1999. Calmodulin supports both inactivation and facilitation of L-type calcium channels. *Nature.* 399:159–162. https://doi.org/10.1038/20200

Zühlke, R.D., G.S. Pitt, R.W. Tsien, and H. Reuter. 2000. Ca2+-sensitive inactivation and facilitation of L-type Ca2+ channels both depend on specific amino acid residues in a consensus calmodulin-binding motif in the(alpha)1C subunit. *J. Biol. Chem.* 275:21121–21129. https://doi.org/10.1074/jbc.M002986200

Supplemental material

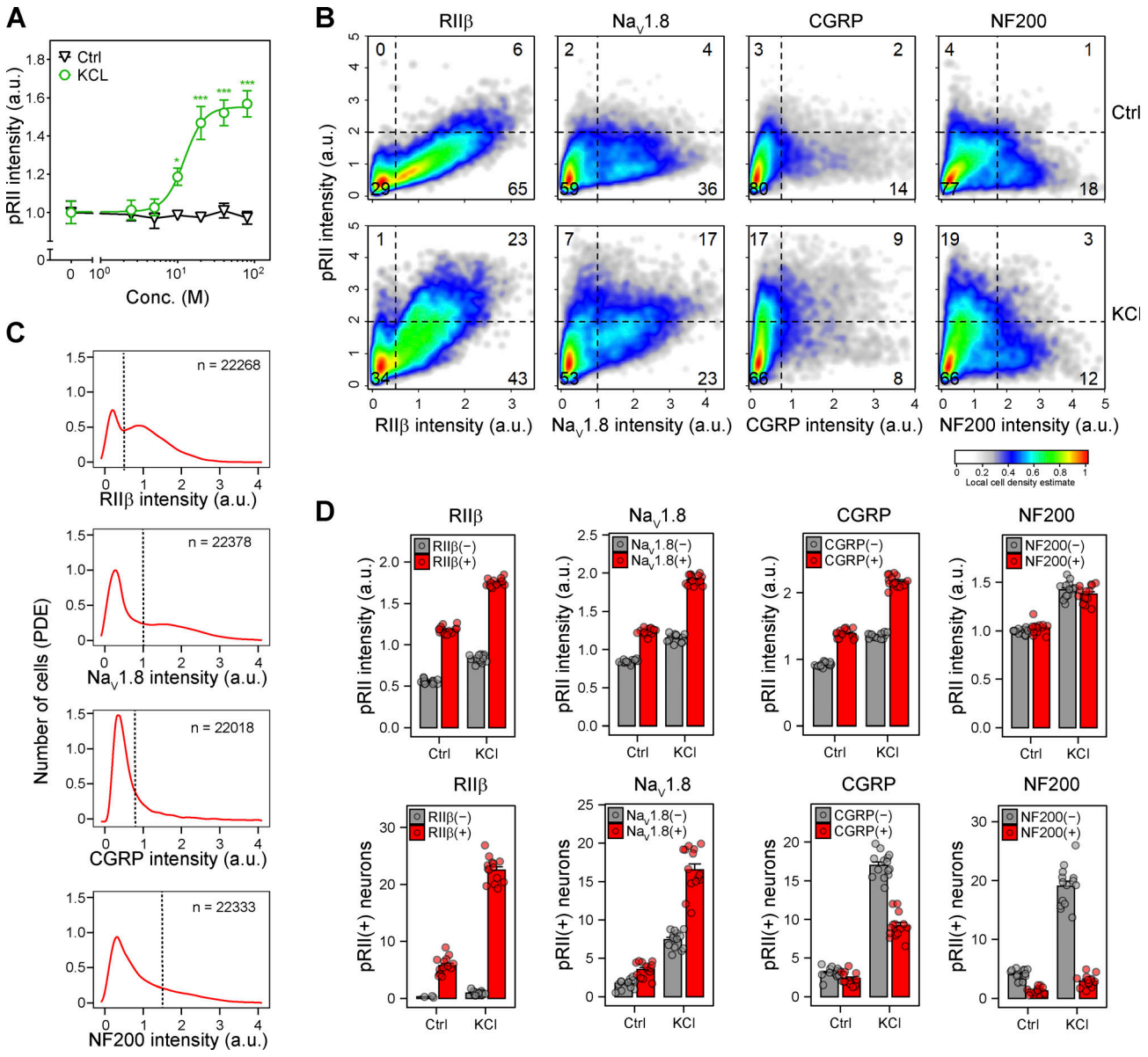

Figure S1. **KCl induces pRII-increase predominantly in nociceptive neurons. (A)** Dose–response curve of pRII intensity in mouse DRG neurons exposed to KCl (0–80 mM, EC_{50} = 10 mM) for 3 min. Data are means ± SEM; *n* = 4 independent experiments; >2,000 neurons/condition; two-way ANOVA with Bonferroni's test; *, P < 0.05; ***, P < 0.001 indicate significance levels between baseline and stimulated conditions. **(B)** Cell density plots of cultured rat DRG neurons labeled for pRII and subgroup markers RIIβ, $Na_V1.8$, CGRP, and NF200. The cells were stimulated with KCl (40 mM, lower panel) or buffer (Ctrl, upper panel) for 3 min to activate PKA-II. Dashed lines indicate gating thresholds used to calculate the percentage of cells in the respective quadrant. Single-cell data of >10,000 neurons per plot from one experiment with pooled cells from *n* = 3 rats are shown. **(C)** Marker intensity distributions used to determine the gating thresholds for the subgroup analysis. **(D)** Quantification pRII intensity and responding pRII(+) neurons in marker-negative and marker-positive neurons from the experiment shown in B and C. Each data point represents the mean of a single culture well.

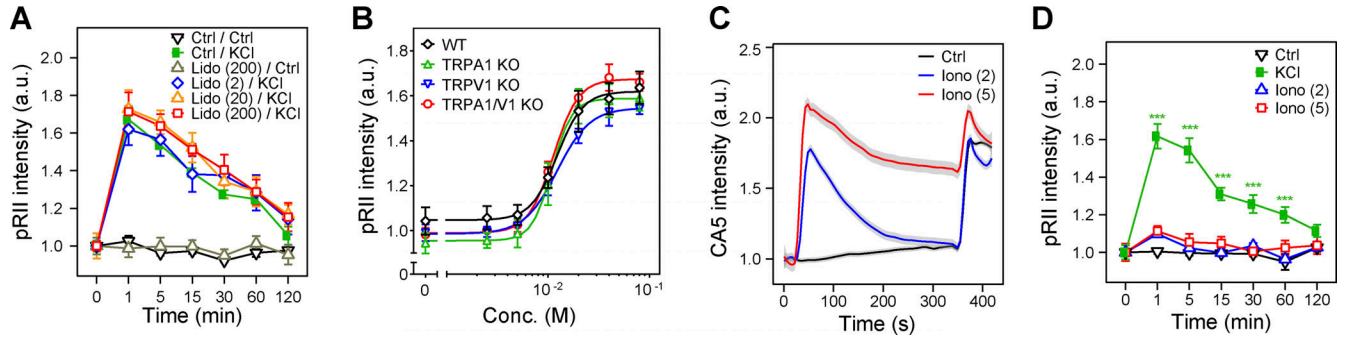

Figure S2. **The increase of pRII intensity induced by KCl is independent of NaV, TRPA1, TRPV1, or ionomycin-induced calcium influx. (A)** Time course of pRII intensity in lidocaine-pretreated (2, 20, and 200 µM; 10 min) rat DRG neurons stimulated with KCl (40 mM). **(B)** Dose–response curve of pRII intensities in DRG neurons of WT, TRPA1, TRPV1, and TRPA1/V1 double-knockout mice exposed to KCl (0–80 mM, EC_{50} = 10 mM) for 3 min. **(C)** Calcium imaging (FLIPR Calcium 5 dye) showing calcium influx evoked by ionomycin (2 or 5 µM) followed by KCl (40 mM). Values in are means ± SEM; *n* = 4; >1,000 neurons/condition. **(D)** Time course of pRII intensities in DRG neurons stimulated with ionomycin (2 or 5 µM) versus KCl (40 mM). Data in A, B, and D are means ± SEM; *n* = 3–4 independent experiments; >2,000 neurons/condition; two-way ANOVA with Bonferroni's test; *, P < 0.05; **, P < 0.01; ***, P < 0.001 indicate significance levels between baseline and stimulated conditions. Calcium imaging data in C are means ± SEM; *n* = 4 independent experiments with a total of >500 analyzed neurons/condition.

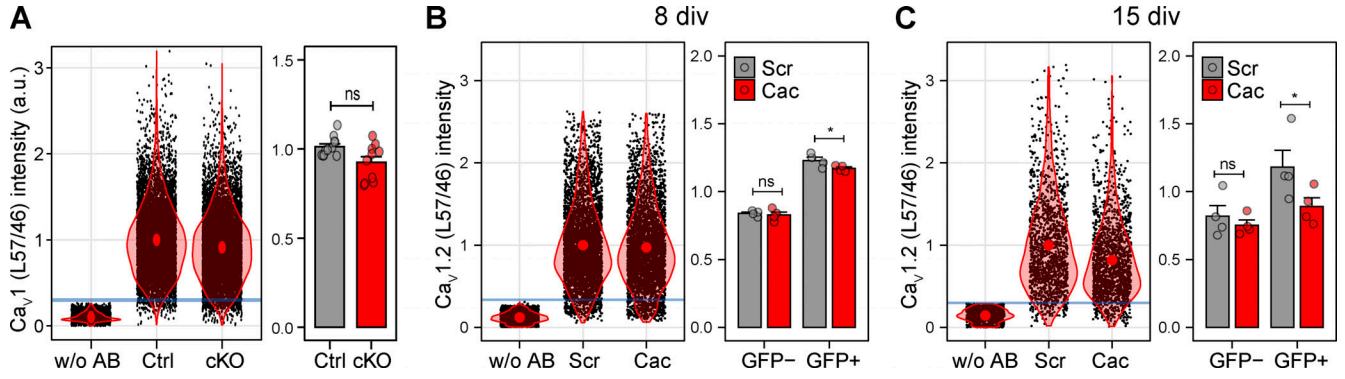

Figure S3. **CaV1-expression in neurons of cKO mice or after AAV-mediated knock down of $Ca_V1.2$. (A)** Single-cell data and mean intensities obtained from Ctrl and cKO mice using a Ca_V1-specific antibody (clone L57/46; *n* = 10 cultures from three mice per genotype, >6,000 neurons per genotype, Student's *t* test). **(B and C)** Single-cell data and mean intensities obtained using a Ca_V1-specific antibody (clone L57/46) at 8 div (B, *n* = 4, >4,000 neurons per condition) and 15 div (C, *n* = 4, >1,500 neurons per condition) after transduction with AAV-PHP.S expressing either a scrambled (Scr) or Cacna1c-specific shRNA, indicating down-regulation of Ca_V1 in GFP^+ neurons. The primary antibody was omitted in respective controls (w/o AB).

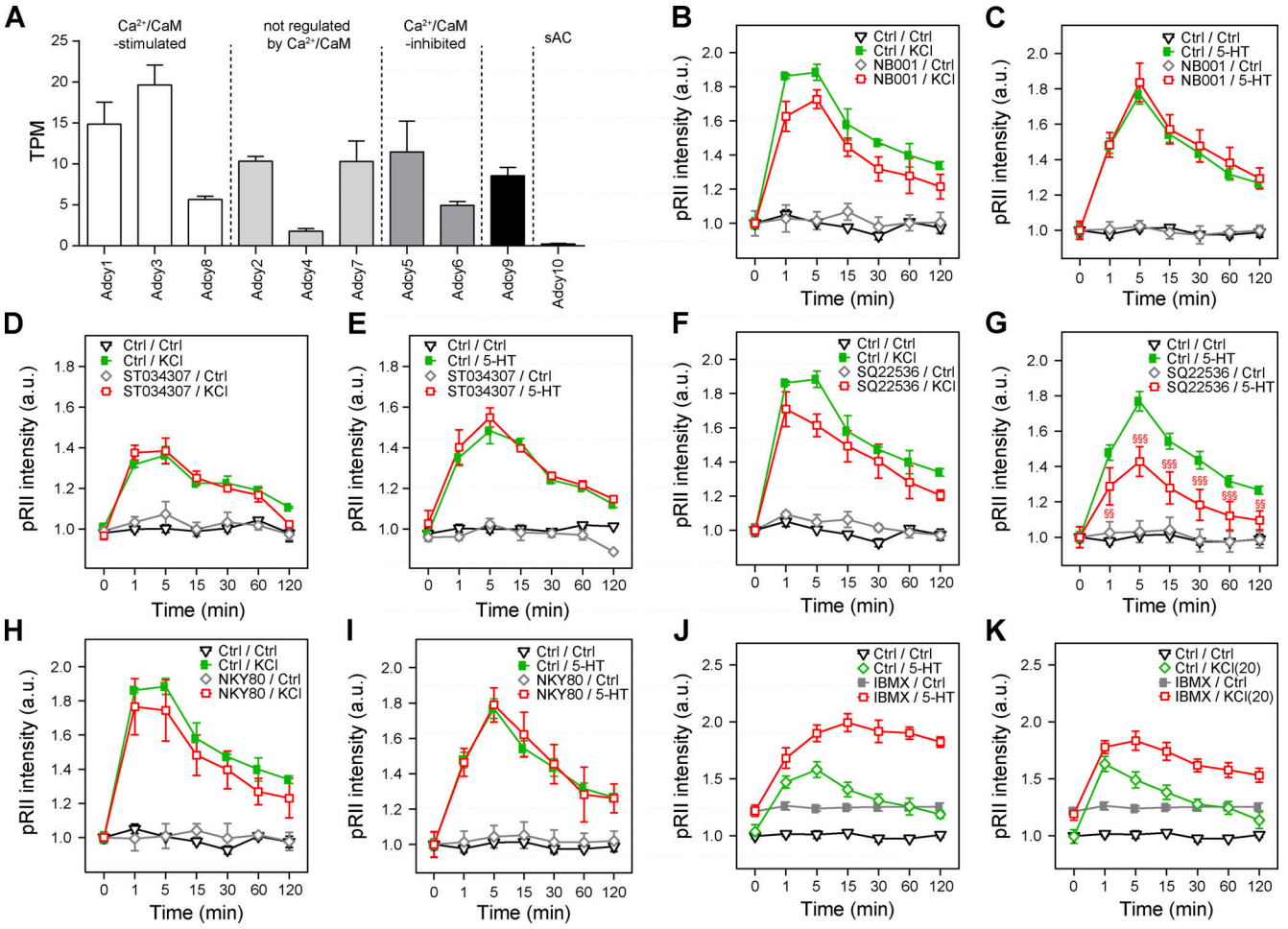

Figure S4. **The KCl-induced increase of pRII intensity cannot be altered by inhibition of adenylycyclases or phosphodiesterases. (A)** Expression pattern of AC isoforms in adult rat DRGs determined by RNA-seq (Isensee et al., 2014b). **(B–I)** Effect of the AC inhibitors NB001, ST034307, SQ22536, and NKY80 (100 µM each, 30-min pretreatment) on the pRII increase induced by KCl (40 mM) or 5-HT (250 nM). **(J and K)** Effect of the phosphodiesterase inhibitor IBMX (100 µM, 30-min pretreatment) on the pRII increase induced by 5-HT (250 nM) or KCl (40 mM). The data shown are not normalized to the baseline difference due to IBMX treatment alone. Data in A are means ± SD, n = 6 replicates. Values in B–K represent means ± SEM; n = 3–4 experiments; >2,000 neurons/condition; two-way ANOVA with Bonferroni's test; §§, $P < 0.01$; §§§, $P < 0.001$ indicate significance levels between 5-HT-induced pRII signals in the absence or presence of an inhibitor.

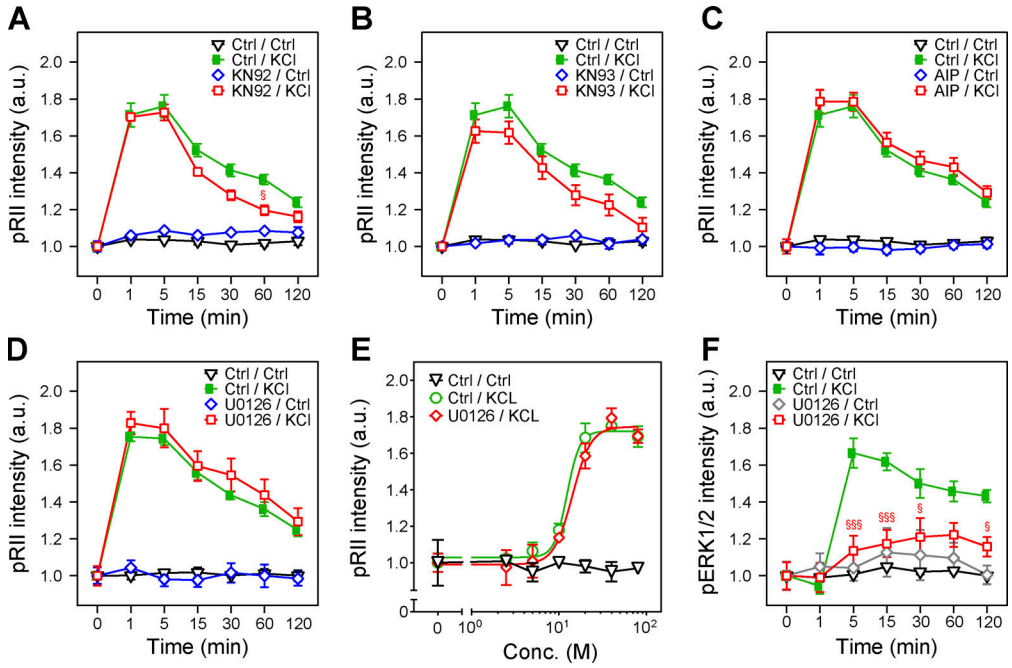

Figure S5. **Neither CaMKII nor MEK inhibitors modulate KCl-induced pRII increases. (A and B)** Effect of the CaMKII inhibitor KN93 (compound effect: $F_{1,42}$ = 16.3, P < 0.0003) and its inactive analogue KN-92 (compound effect: $F_{1,42}$ = 17, P < 0.0002; 10 µM each, 30-min pretreatment) on the pRII increase induced by KCl (40 mM). **(C)** Exposure to AIP (1 µM, 30 min) is not inhibiting the pRII response to KCl (40 mM). **(D)** Exposure to the ERK1/2 inhibitor U0126 (1 µM, 30 min) is not inhibiting the pRII response to KCl (40 mM). **(E)** Dose–response of KCl (0–80 mM) in the absence or presence of U0126 (1 µM, 30 min). **(F)** The MEK inhibitor U0126 (1 µM, 30 min) prevents the pERK1/2 increase after KCl depolarization. Values represent means ± SEM; *n* = 3–4 experiments; >2,000 neurons/condition; two-way ANOVA with Bonferroni's test; §, P < 0.05; §§§, P < 0.001 indicate significance levels between KCl-induced pRII signals in the absence or presence of an inhibitor.